



Direct investigation of methane nanofluidic microstructure and system dynamics in rough silicon nanochannel

Chuntao Jiang¹ · Qingsheng Liu¹ · Xuehai Wang¹

Received: 10 November 2018 / Accepted: 26 September 2019 / Published online: 11 October 2019
© Springer-Verlag GmbH Germany, part of Springer Nature 2019

Abstract

The microstructure and system dynamics of methane nanofluidic are important to determine the flow properties. In this study, we use non-equilibrium multiscale molecular dynamics simulation (NEMSMD) to investigate the microstructure and system dynamics of methane nanofluidic confined by rough silicon atomic walls. To capture the detailed atomic microstructure of methane moving in rough nanochannel accurately, the modification of OPLS methane fully atomic model is employed. The average number density distributions of C (H) atom, average velocity profile, velocity autocorrelation function and projection radial distribution function (XOY-, XOZ- and YOZ planes) plots give a clear observation of the impacts of different conditions (roughness, body driving force, fluid–wall interaction strength and cutoff radius) on the methane Poiseuille flow in nanochannel. The projection radial distribution functions and diffusivity appear anisotropic, and seem to be affected more significantly by roughness, fluid–wall interaction strength and cutoff radius than body driving force in the whole channel region. Moreover, the body driving force and cutoff radius also play an important role in methane nanofluidic simulation using NEMSMD. The present simulation results are very meaningful for the design of energy-saving emission reduction nanofluidic devices.

Keywords Multiscale · Molecular dynamics · Projection radial distribution functions · Poiseuille flow · Diffusivity

1 Introduction

Over the recent decades, the micro- and nanochannel flows have attracted significant scientific and industrial interest, because of the need of optimal design for micro- and nanofluidic devices and fabrication of small-scale systems, such as water desalination (Corry 2008), nano-filtration systems (Wang et al. 2015), CO₂ separation and storage (Mantzalis et al. 2011), nanomedicine (Hare et al. 2016), nanomanufacturing and environmental sciences (Li et al. 2016), and many more, as reviewed in literature (Cao et al. 2009; Sundar et al. 2017). In the nanoscale, since experimental studies are very difficult to perform, atomistic dynamic simulation techniques provide the means for exploring physical space and time space. Especially, at the boundary between nanochannel wall atoms and fluid molecules, most fluid properties are affected by the fluid–wall interaction strength, and the

precise description of phenomena occurring at these interfaces becomes very important in nanochannel (Cao et al. 2006a, b, 2009; Duan et al. 2015; Karniadakis et al. 2006).

To understand the atomic processes of fluids occurring at the rough solid interface, various MD studies have been presented in the literature with respect to effects of surface properties, such as roughness of nanochannel surfaces, wettability and the slip (Cao et al. 2006a, b; Jiang et al. 2016a, 2017a, b; Sofos et al. 2009a, b, 2010). However, there are still numerous problems to be resolved. First, at the atomic level, how to describe the roughness of nanochannel wall is the urgent need to be addressed (Cao et al. 2009; Karniadakis et al. 2006; Mantzalis et al. 2011). Second, the fluid–wall interaction strength does not reach a consensus for the complex atomistic fluids through the rough nanochannel surface. Besides, the microstructure and system dynamics of nanofluidic should also be studied in detail, because it determines the nanofluidic properties (Jiang et al. 2017c; Markestijn et al. 2012; Mashayak and Aluru 2012b; Sharma et al. 2016; Sofos et al. 2012).

The roughness of nanochannel surface has significant effects on the flow properties and detailed atomic

✉ Chuntao Jiang
chuntao118@163.com

¹ School of Mathematics and Statistics, Xinyang Normal University, Xinyang 46400, China

microstructure of liquid flows. Although several classical rough wall patterns have been available in the literature (Cao et al. 2006a, b; Jabbarzadeh et al. 2000; Kim and Strachan 2015; Mo and Rosenberger 1990; Noorian et al. 2014; Priezjev 2007), there is no an appropriate theory to describe the characterization of realistic surface roughness (Cao et al. 2009). Jabbarzadeh et al. showed that the slip length of liquid hexadecane increases at near sinusoidal-wall with the increase of the roughness period (Jabbarzadeh et al. 2000). Mo and Rosenberger studied the effects of sinusoidally and randomly roughened wall on momentum transfer of gas argon (Mo and Rosenberger 1990). Later, Noorian et al. studied the effect of wall roughness on the liquid argon moving in the randomly and periodically roughened nanochannel wall via the NEMD simulations (Noorian et al. 2014). Priezjev defined randomly and periodically roughened surface, and researched the relation between slip length and roughness amplitude (Priezjev 2007). Kim and Strachan investigated the impacts of the roughness on squeeze-film damping for random and periodical surfaces (Kim and Strachan 2015). However, these wall patterns can not quantitatively measure the roughness of nanochannel surfaces. Meantime, some researchers depicted the roughness of nanochannel surfaces using the periodical and rectangular waves (Cao et al. 2006a, b, 2009; Jiang et al. 2016b, 2017a, c; Sofos et al. 2009a, b, 2010, 2012, 2016; Zhang 2016a, b). Cao et al. reported that the velocity values of gaseous argon decrease with increasing amplitude near the rough platinum atom wall (Cao et al. 2006a, b, 2009). Sofos et al. investigated the effects of roughness on the liquid argon through krypton nanochannel systematically (Sofos et al. 2009a, b, 2010, 2012, 2016). Zhang used the flow factor approach model to study the effects of the surface roughness on the fluid mass flow rate through a nano-slit pore (Zhang 2016a, b). Jiang et al. developed the NEMSMD method to investigate the properties of methane nanofluidic moving the rough nanochannel walls (Jiang et al. 2017a, c).

Considering the fluid–wall interaction strength, previous research mainly employed the LJ (12-6) potential function to describe fluid–wall interaction (Cao et al. 2006a, b, 2009; Kim and Darve 2006; Priezjev 2007; Sofos et al. 2009a, b, 2010, 2016), and the parameters of potential calculated by classical Lorentz–Berthelot (L–B) mixing rule ($\epsilon_{\text{FW}} = \sqrt{\epsilon_{\text{F}} \cdot \epsilon_{\text{W}}}$, $\sigma_{\text{FW}} = (\sigma_{\text{F}} + \sigma_{\text{W}})/2$) for simple argon fluid moving platinum or krypton walls. For the complex water molecules through the silicon atom nanochannel walls, Markesteijn et al. suggested using between oxygen and silicon atoms interaction to solve the problem of water molecule and silicon interaction. The hydrogen and silicon atoms interactions are ignored (Markesteijn et al. 2012). Mashayak and Aluru utilized the coarse-grained (CG) model to deal with the fluid–wall interaction for the prediction structure of water confined by grapheme (silicon) nanochannel. However, the

coupling between the potential parameters makes it even more difficult (Mashayak and Aluru 2012a, b). To solve the fluid–wall interaction problem in studying the methane through the silicon atom nanochannel walls, we presented the NEMSMD simulation method and applied it to investigate the viscosity, local transfer mass and the other micro-properties in the rough nanochannel walls successfully (Jiang et al. 2016b, 2017a, c). The merit of NEMSMD method is that the fluid–wall interaction strength is obtained from the CG methane models via coupling the L–B mixing rule (Kong 1973). The CG potential parameters are optimized by relative entropy minimization method (Shell 2008). Moreover, the wall–CG interaction strength is close to realistic fluid–wall interaction, because the potential of mean force of CG model is in good agreement with the corresponding fully atomistic model ($W(r) = -k_{\text{B}}T \ln g(r)$) (Jiang et al. 2017b, c; Noid 2013). At the same time, the NEMSMD simulation can be utilized not only to solve the physical boundary problem but also to capture the micro atom (C and H atom) information of methane nanofluidics. Besides, this method can be used to study other complex molecules fluid moving the atom nanochannel. For these reasons, the NEMSMD method is very suitable for investigating the effect of wall roughness on the microstructure characteristics and system dynamics of complex methane fluid moving the rough nanochannel walls.

To the best of our knowledge, detailed reporting of microstructure properties and system dynamics for methane nanofluidic appears to be rare in the literature. The primary goal of this work is to investigate the influence of the wall roughness (fluid–wall interaction, body driving force and cutoff radius) on microstructure and system dynamics for methane Poiseuille flow in nanochannel using NEMSMD simulation. To exhibit the advantage of NEMSMD in studying the effect of different simulation conditions on the fluid atom behavior and microstructure properties, C (H) atom number density distribution and detailed projection radial distribution functions [$g_{\text{CC}}(r)$, $g_{\text{CH}}(r)$ and $g_{\text{HH}}(r)$] on three coordinate planes are discussed. To demonstrate the system dynamics of methane nanofluidic and the average velocity profile, diffusion coefficients are investigated by altering the roughness, fluid–wall interaction, body driving force and cutoff radius.

The rest of this paper is organized as follows. In Sect. 2, our models and simulation method are given. Next, numerical results are shown and discussed in Sect. 3. Finally, we present conclusions from this study and show some directions for future work in Sect. 4.

2 Models and simulation details

The NEMSMD simulation is employed to study the microstructure characteristic and dynamics properties for methane nanofluidic confined by the rough silicon atomic wall at

a given distance in the z -direction. The nanochannel model itself is created by placing two parallel silicon atoms in an ABAB stacking (Kamal et al. 2013). Between the two rough silicon walls, the methane molecules are organized as a face-centered cubic lattice, with an initial thermodynamic state point density $\rho = 377.15 \text{ kg/m}^3$ and corresponds to $T = 140 \text{ K}$, $P = 1.525 \text{ MPa}$.

In nanoscale, the roughness plays an important role in the research of the microstructure and system dynamics of the nanofluidic. In order to do a quantitative analysis of the wall roughness, the rough nanochannel walls are described by “anchoring” extra wall atoms on smooth atom wall to form periodically rectangular wave with different amplitudes and wavelengths, and each wall is composed of four layers of silicon atoms (each layer consisting of 240 silicon atoms); the height of the surface should vary with lateral position. For simplicity, the “anchoring” extra wall atoms are displaced by $\Delta z(x)$ according to the following expressions for the nanochannel surfaces:

$$\Delta z(x) = \begin{cases} 2A_i, & 0 < x \leq \lambda_j/2, \\ 0, & \lambda_j/2 < x \leq \lambda_j, \end{cases} \quad (1)$$

where A_i and λ_j are characteristics of the roughness, respectively, representing the amplitude and wavelength of the periodically rectangular wave nanochannel walls. In this work, we consider a given amplitude and three wavelengths for the periodic roughness of walls, and show it in Fig. 1. The periodic boundary conditions are employed in the x - and y -directions in all cases, while in the z -direction, the realistic solid physical boundary condition was used, and separation of the wall atoms is large enough for methane molecular fluids to penetrate beyond the wall surface layers.

Moreover, the length of the simulation box in the x -direction should be chosen in such a way that it accommodates an integer number of full rectangular wave depending on the wavelength λ_j ($i = 1, 2, 3$). In fact, our selected simulation system consists of 1560 (λ_i, A) ($i = 1, 2, 3$) fluid methane molecules with different rough walls, and bounded by 2400 silicon atoms wall which are subjected to an additional harmonic potential with respect to an ABAB stacking (Kamal et al. 2013) (see from Fig. 1) site \mathbf{r}_{eq} ,

$$u\left(\left|\mathbf{r}(t) - \mathbf{r}_{\text{eq}}\right|\right) = \frac{1}{2}k_w \left(\left|\mathbf{r}(t) - \mathbf{r}_{\text{eq}}\right|\right)^2, \quad (2)$$

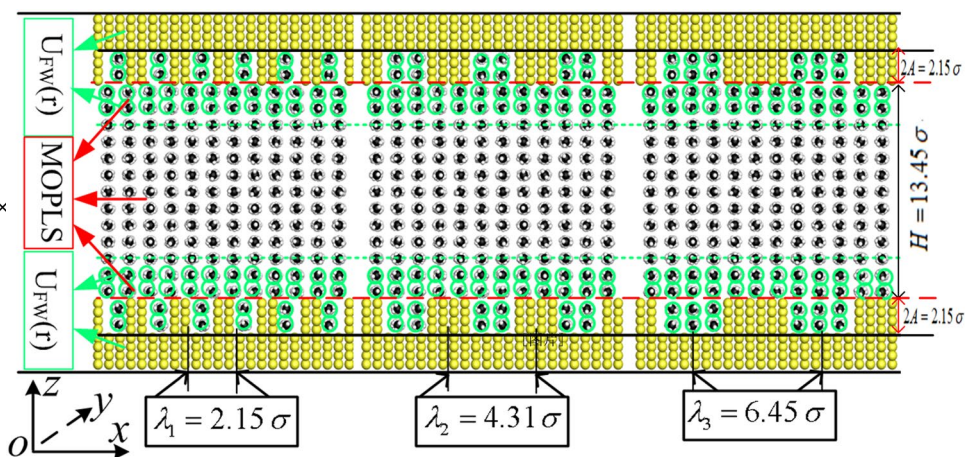
where $\mathbf{r}(t)$ is the position of a boundary particle at time t . The rigidity of the wall is determined by the force constant k_w and the value used ($72\epsilon_S/(2^{1/3}\sigma_S^2)$) is obtained by computing $r = r_0 = 2^{1/6}\sigma_S$ in the second derivative of the interaction LJ (12–6) potential of silicon atoms (Kamal et al. 2013), where the parameters are $\sigma_S = 3.826 \text{ \AA}$, $\epsilon_S = 1.6885 \text{ kJ/mol}$, and the density of silicon is 2329 kg/m^3 (Hu et al. 2015).

The modification of OPLS (MOPLS) model was given by Jiang et al. for studying the structure and transport properties of dense methane fluid at the low temperature domains (Jiang et al. 2017c). The potential function of fully atomistic methane model is given as

$$U(r) = \sum_{\alpha, \beta} \sum_{i \in \alpha, j \in \beta} \left(4\epsilon_{\text{ab}} \left(\left(\sigma_{\text{ab}}/r_{ij} \right)^{12} - \left(\sigma_{\text{ab}}/r_{ij} \right)^6 \right) + q_i q_j / 4\pi\epsilon_0 r_{ij} \right), \quad (3)$$

where ϵ_0 , ϵ , σ , q and r_{ij} denote the vacuum permittivity, interaction energy well depth, length scale, point charge and the distance between atoms i and j , respectively. Subscripts α and β are used to distinguish the interactions between

Fig. 1 Schematic of the interactions of fluid–fluid and fluid–wall using non-equilibrium MSMD simulations. The roughness and the high of nanochannel are given. Channel dimensions are $L_x \times L_y \times L_z = 12.4 \sigma \times 10.3 \sigma \times (\sigma = 4.01 \text{ \AA}, L_z = H + 4A)$



different molecules, a and b represent different types atoms (C and H). The bond length of C–H is $l_{CH} = 1.087 \text{ \AA}$ in MOPLS model. The charges are $q_C = -4q_H = -0.572 e$ in the potential function. All the parameters of MOPLS are given in Table 1.

In this study, the CGMOPLS model coupled with L–B mixing rule is employed to solve the problem of the fluid–wall interaction (see Fig. 1) rather than simply ignoring the charge force and H atom interaction near the wall ($\leq r_{cut}$) (Jiang et al. 2017a, c). Moreover, the LJ interatomic pair potential is commonly used in MD simulations of solid–liquid boundaries, because the potential function of solid silicon atom is LJ (12–6) potential (Kamal et al. 2013). The potential function of fluid–wall interaction is given as follows:

$$U_{FW} = 4\epsilon_{FW} \left(\left(\frac{\sigma_{FW}}{r} \right)^{12} - \left(\frac{\sigma_{FW}}{r} \right)^6 \right). \tag{4}$$

The parameters of fluid–wall σ_{FW} and ϵ_{FW} for methane–silicon interactions are calculated by the classical L–B mixing rule (Kong 1973)

$$\epsilon_{MS} = \chi \sqrt{\epsilon_{CG} \cdot \epsilon_S}, \quad \sigma_{MS} = (\sigma_{CG} + \sigma_S)/2 \tag{5}$$

where χ is the potential energy factor indicating the strength of hydrophilic interaction. To investigate the effect of the strength of hydrophilic interaction on structural properties and system dynamics of methane nanofluidics, $\chi = \{0.5, 1.0, 1.5\}$ are employed. The interaction of methane CG particles is implicitly incorporated into the effective pair interaction potential given as

$$U_{CG} = 4\epsilon_{CG} \left(\left(\frac{\sigma_{CG}}{r} \right)^{12} - \left(\frac{\sigma_{CG}}{r} \right)^6 \right). \tag{6}$$

The parameters of CG potential are determined by the relative entropy minimization method (Jiang et al. 2017b; Shell 2008) in the bulk methane fluid under NVT ensemble. The obtained parameters of the CG potential are $\sigma_{CG} = 3.645 \text{ \AA}$, $\epsilon_{CG} = 1.329 \text{ kJ/mol}$ at the $\rho = 377.15 \text{ kg/m}^3$ and $T = 140 \text{ K}$. The potential of mean force ($W(r) = -k_B T \ln g(r)$) and radial distribution function of CG model are in better agreement with the corresponding fully atomistic model than unit atom LJ model (Jiang et al. 2017a, b; Noid 2013). It indicates that we can

obtain the ideal fluid–wall interaction by the classical L–B mixing rule coupling the corresponding CG model. The relevant results can be seen in our previous research work (Jiang et al. 2016b, 2017a, b, c).

To avoid compressibility effects, the body driving force $f_{ex} = 0.075 (\epsilon/\sigma \approx 0.4919 \times 10^{-12} \text{ N})$ is applied along the x -direction to drive the flow for different roughness of nanochannel walls (fluid–wall interaction strength and cutoff radius) (Jiang et al. 2016b). And the body driving forces ($f_{ex} = \{0.05, 0.075, 0.1, 0.125\} \epsilon/\sigma$) are selected to study its influence on the methane Poiseuille flow in rough nanochannel surfaces. All interactions of intermolecular are subject to a continuous force (or continuous energy) cutoff radius of $r_{cut} = 2.5 \sigma$ (for roughness, fluid–wall interaction strength and body driving force). The orientational coordinates of the methane tetrahedral are expressed in terms of quaternion parameters; the mass center motion of molecules is calculated via the fifth Predictor–Corrector method (Rapaport 2004). To control the temperature of system, the NVT ensemble with Nosé–Hoover thermostat is employed. Whether the thermostat follows the equipartition theorem is checked, by comparing the thermal kinetic energy per methane molecules in y - and z -directions

$$mv_y^2/2 = k_B T/2, \tag{7}$$

$$mv_z^2/2 = k_B T/2, \tag{8}$$

where m , k_B , T , v_y and v_z denote the mass of molecule, Boltzmann constant, temperature, velocity of y - and z -directions, respectively. This can ensure that the thermostat effect is observed in each direction due to the interactions of intermolecular, despite x -direction is not explicitly considered (Bhadauria and Aluru 2013). The scaling parameters are $\sigma = 4.01 \text{ \AA}$ and $\epsilon/k_B = 142.87 \text{ K}$. The time step $\Delta t = 1.3 \times 10^{-15} \text{ s}$ is utilized. The first 2.0×10^5 MD time steps were discarded and the relevant information was obtained from further 5.0×10^5 time steps. The average streaming velocity profiles and atom (C and H) distributions profiles are collected by dividing different roughness with wavelength values (λ_i ($i = 1, 2, 3$)) in 400 bins. The averaged velocity profiles are calculated by

$$v_x(z) = \left\langle \frac{\sum_{i=1}^{N_{bin}} v_{x,i}(z, z+h_{bin})}{N_{bin}(z, z+h_{bin})} \right\rangle, \tag{9}$$

and the C and H atom number density distribution profiles are calculated by

$$N_{C/H}(z) = \frac{\langle N_{bin,C/H}(z, z+h_{bin}) \rangle}{\bar{N}}, \tag{10}$$

Table 1 The potential parameters of fully atomic methane model used in this study (Jiang et al. 2016b)

Type	Parameter	C–C	C–H	H–H
MOPLS	ϵ/k_B (K)	46.8	17.17	6.30
	σ (\AA)	3.45	3.06	2.67

where N_{bin} is the number of methane molecules in $[z, z + h_{bin})$, \bar{N} is the corresponding averaged number density of fluid atoms (C and H) in the whole channel, and $\langle \cdot \rangle$ denotes the ensemble average. To study the system dynamics, the velocity autocorrelation function is obtained from Rapaport (2004)

$$C_V(t) = \frac{1}{N} \left\langle \sum_{i=0}^{N-1} (\mathbf{v}_i(0) \cdot \mathbf{v}_i(t)) \right\rangle. \tag{11}$$

Diffusivity is a significant system dynamic characteristics of the nanofluidic, for excluding the influence of macroscopic flow velocity on the diffusivity, diffusion coefficient value is calculated using the amendment Green–Kubo relations (Bitsanis et al. 1987)

$$D = \frac{1}{3N} \int_0^\infty \left\langle \sum_{j=0}^{N-1} (\mathbf{v}_j(0) - \bar{\mathbf{v}}) \cdot (\mathbf{v}_j(t) - \bar{\mathbf{v}}) \right\rangle dt, \tag{12}$$

where N , $\mathbf{v}_i(0)$, $\mathbf{v}_i(t)$ and $\bar{\mathbf{v}}$ denote the number of fluid molecule, the velocity of the j th molecule at time 0, the velocity of the j th molecule at time t and flow velocity, respectively.

The structural properties are very important in most nanofluidic systems. The radial distribution function is a basic measure of the structure of a fluid. It measures the probability density of finding a particle at a distance r from a given particle position. The radial distribution function is defined by

$$g(\mathbf{r}) = \frac{1}{\rho N} \left\langle \sum_{i=1}^N \sum_{j=1, j \neq i}^N \delta(\mathbf{r} - \mathbf{r}_{ij}) \right\rangle, \tag{13}$$

where N and $\rho = N/V$ denote the total number of particles and the number density, respectively. The angular brackets represent a time average. The value of the δ -symbol is equal to one while $\mathbf{r} = \mathbf{r}_{ij}$, otherwise is zero. To better explore the structural properties of methane Poiseuille flow in nanochannel, the projection radial distribution functions are evaluated as local values on three planes (XOY, XOZ and YOZ). To obtain these results, the fluid domain is divided into $n_x \times n_y \times n_z = (240 \times 200 \times 340)$ bins inside the whole channel. And the number density ($\rho = N/V$) is replaced by the planes number density ($\rho = N/(L_1 \times L_2)$, 1, 2 denote x , y or z) in calculating the projection radial distribution function. All the simulation program codes are developed using C++ on windows operating systems (Rapaport 2004).

3 Results and discussion

In this work, we mainly discuss the impacts of roughness, fluid–wall interaction strength, body driving force and cutoff radius on the microstructure and system dynamics of methane nanochannel flow.

3.1 Roughness

To explore the effects of wall roughness on the microstructure and system dynamics of methane nanofluidic, three nanochannel walls (see Fig. 1) are selected in this study. The total average number density distribution profiles of C and H atoms are shown in Fig. 2. In the central part of the nanochannel regions, the atoms (C and H) number density is larger for $\lambda_1 = 2.15 \sigma$, and the atoms' (C and H) number density is the smallest for $\lambda_2 = 4.31 \sigma$. Inside the cavities, all peak values of atoms (C and H) number density for $\lambda_2 = 4.31 \sigma$ are obviously bigger than that of the other wavelength ($\lambda_1 = 2.15 \sigma$, $\lambda_3 = 6.45 \sigma$). Moreover, the peak value of H atom number density is obviously lower than that of C atom, and the peak width of H atom number density is wider than that of C atom. The opposite conclusions can be obtained from the minimum values and valley width of the atoms (C and H) number density distribution for all wavelengths. Near the rough wall regions, we observe that the atoms (C and H) number density distribution presents various variations with the change of wavelength. The numerical results display that the C (H) atom number density distribution of methane molecule depends on the roughness of nanochannel at near wall. Besides, the anisotropy of methane

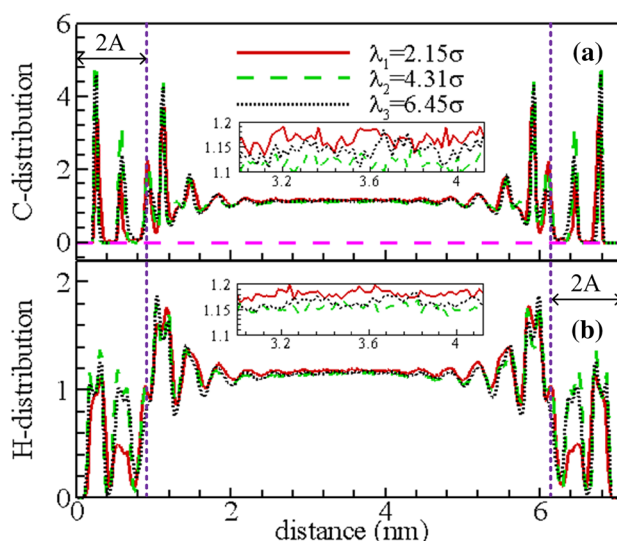


Fig. 2 Total average C-distribution and H-distribution profiles plotted for different roughness over the whole channel region

molecule increases with the increasing the wavelengths near nanochannel walls. All the numerical results indicate that the observed H atom (C atom) frequency becomes low (high) in the bins. It may be attributed to the fact that the translational mobility or rotary movement of methane becomes slow near nanochannel wall and inside cavity (Jiang et al. 2017c). The results are similar to the research of Sofos et al. for liquid argon through krypton nanochannel (Sofos et al. 2009b). It indicates that the fluid atom localization inside the cavities increases while the protrusion length decreases, i.e., the roughness of wall has a major influence on the fluid atom localization distribution.

The total average streaming velocity profiles in time and space are given in Fig. 3 for different rough nanochannel walls. The average streaming velocity profiles obtained from the NEMSMD simulations are similar to the Poiseuille flow velocity profile, with slight differences near the walls. It indicates that the mainstream regime of the methane nanofluidic through the rough nanochannel obeys the continuum mechanics characterized by the Navier–Stokes equation. The velocity values fluctuate adjacent to the rough nanochannel walls, which denote the molecules suffered from the resistance force of protrusion while they are confined to the cavities. The values of maximum velocity slightly change as the wavelength is no less than 4.31σ . When $\lambda_1 = 2.15 \sigma$, the maximum value of velocity is obviously smaller than other two values, indicating that the effect of wall roughness on the mobility of molecule is significant at small wavelength. Moreover, the values of velocity in cavities and near rough walls present an irregular fluctuation, which is attributed to the complex fluid–wall interaction force in the cavities or near the wall. These results denote that the roughness of wall has an impact on the mobility of fluid molecule.

To investigate the effects of roughness on the system dynamic properties of methane nanofluidic, the normalized velocity autocorrelation functions are shown in Fig. 4a. It is

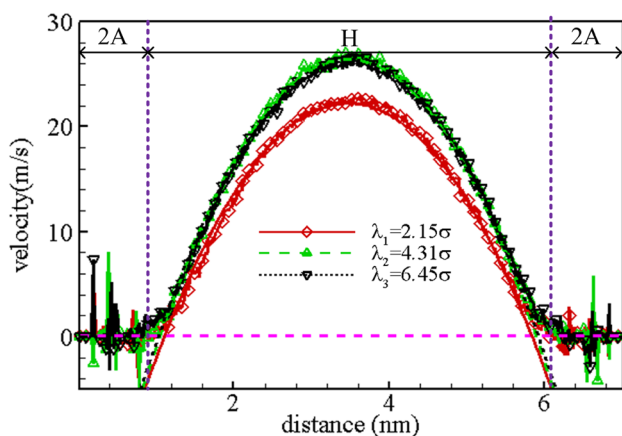


Fig. 3 Total average streaming velocity profiles plotted for different roughness over the whole channel region

clear that all the normalized velocity autocorrelation functions reach a plateau value at about $t = 0.90$ ps. And the time (normalized velocity autocorrelation functions value approximates to zero) decreases with the increasing wavelength. For $\lambda_1 = 2.15 \sigma$, the normalized velocity autocorrelation function presents periodic oscillations, which are attributed to the methane molecules presented periodic rotating vibration and many collisions with wall atoms inside the cavities. Besides, we can see from Fig. 4a that the frequency oscillations of normalized velocity autocorrelation functions rapidly disappear as the wavelength is not less than 4.31σ . The disparity in the normalized velocity autocorrelation function is attributed to the trajectories of molecules obtained from different roughness. To further explore the reason of period phenomenon of normalized velocity autocorrelation function, we plot normalized velocity autocorrelation function for the x -, y - and z -directions in Fig. 4b. The calculated results indicate the back and forth movement of molecules (inside cavities) in x -direction. The diversity of normalized velocity autocorrelation function between y - and z -direction is due to the boundary condition. Actually, the diffusion coefficient, being proportional to single particle correlations in pure fluids, is the transport coefficient most reliably extracted from the molecular trajectories. We calculated the diffusion coefficients: $71.05 \pm 1.37 (10^{-10} \text{ m}^2 \text{ s}^{-1})$, $76.27 \pm 0.56 (10^{-10} \text{ m}^2 \text{ s}^{-1})$ and $77.77 \pm 0.91 (10^{-10} \text{ m}^2 \text{ s}^{-1})$ for $\lambda_1 = 2.15 \sigma$, $\lambda_2 = 4.31 \sigma$ and $\lambda_3 = 6.45 \sigma$ in the whole nanochannel, respectively. These results show that the diffusion coefficients increase with the increasing rough wavelength. Meantime, the diffusion coefficients of different directions (for $\lambda_1 = 2.15 \sigma$) are given as: $D_x = 68.42 \pm 0.97 (10^{-10} \text{ m}^2 \text{ s}^{-1})$, $D_y = 77.52 \pm 1.23 (10^{-10} \text{ m}^2 \text{ s}^{-1})$ and $D_z = 67.37 \pm 1.48 (10^{-10} \text{ m}^2 \text{ s}^{-1})$.

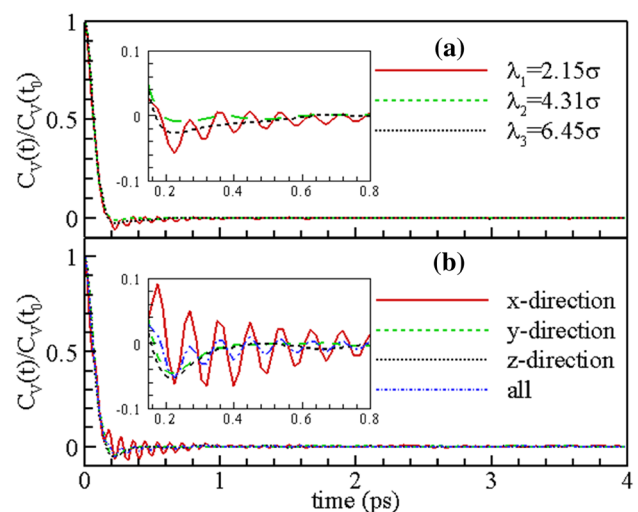


Fig. 4 The normalized velocity autocorrelation function plotted for different roughness over the whole channel region

These present results mean that there is always anisotropy in diffusion coefficient of methane nanofluidic moving rough nanochannel. This can be attributed to the fact that the different rough wavelengths effect is strong for fluid mobility in rough nanochannel. Especially, when the methane molecules are adjacent to the walls ($\leq r_{cut}$), they suffer from the interaction of the other methane molecules via using MOPLS model [$U(r_{ij})$] and wall atoms by the fluid–wall interaction potential function [$U_{MS}(r_{ij})$].

So as to clearly study the structure information of methane nanofluidic flowing different rough nanochannels, calculation of the projection radial distribution function [$g_{CC}(r)$, $g_{CH}(r)$ and $g_{HH}(r)$] has been performed in two ways: curve and contour. At first, we consider the radial distribution function [$g_{CC}(r)$, $g_{CH}(r)$ and $g_{HH}(r)$] projections on three planes (XOY, XOZ and YOZ) by curve in the whole

nanochannel. For different rough nanochannels, these results are shown in Figs. 5a₁–a₃, 6a₁–a₃ and 7a₁–a₃ for XOY-, XOZ- and YOZ planes, respectively. The first and second peak values of radial distribution functions [$g_{CC}(r)$, $g_{CH}(r)$ and $g_{HH}(r)$] present various variations with the change of wavelength in three planes. Concretely speaking, in XOY plane, the first peak value coordinates of C-atom radial distribution functions are (1.024, 4.008), (1.024, 7.194) and (1.006, 5.866) for λ_1 , λ_2 and λ_3 , respectively. Although this result does not show some regularity, it indicates the rough wavelength impacts on the structure properties of methane nanofluidic. And we observe that the C-atom radial distribution function has an obvious difference around distance ($= 2\sigma$). The difference can be clearly seen from Fig. 5b₁–b₃, which plots contour of C-atom radial distribution function project on the XOY plane. Moreover, the contour of atom

Fig. 5 a₁–a₃ Total average projections of the radial distribution function [$g_{CC}(r)$, $g_{CH}(r)$ and $g_{HH}(r)$] plotted over the whole channel region in XOY plane with different roughness. The contours of radial distribution function [$g_{CC}(r)$, $g_{CH}(r)$ and $g_{HH}(r)$] projected onto XOY plane for [b₁–b₃: $g_{CC}(r)$, c₁–c₃: $g_{CH}(r)$ and d₁–d₃: $g_{HH}(r)$] plotted for different periodic roughness of nanochannel walls

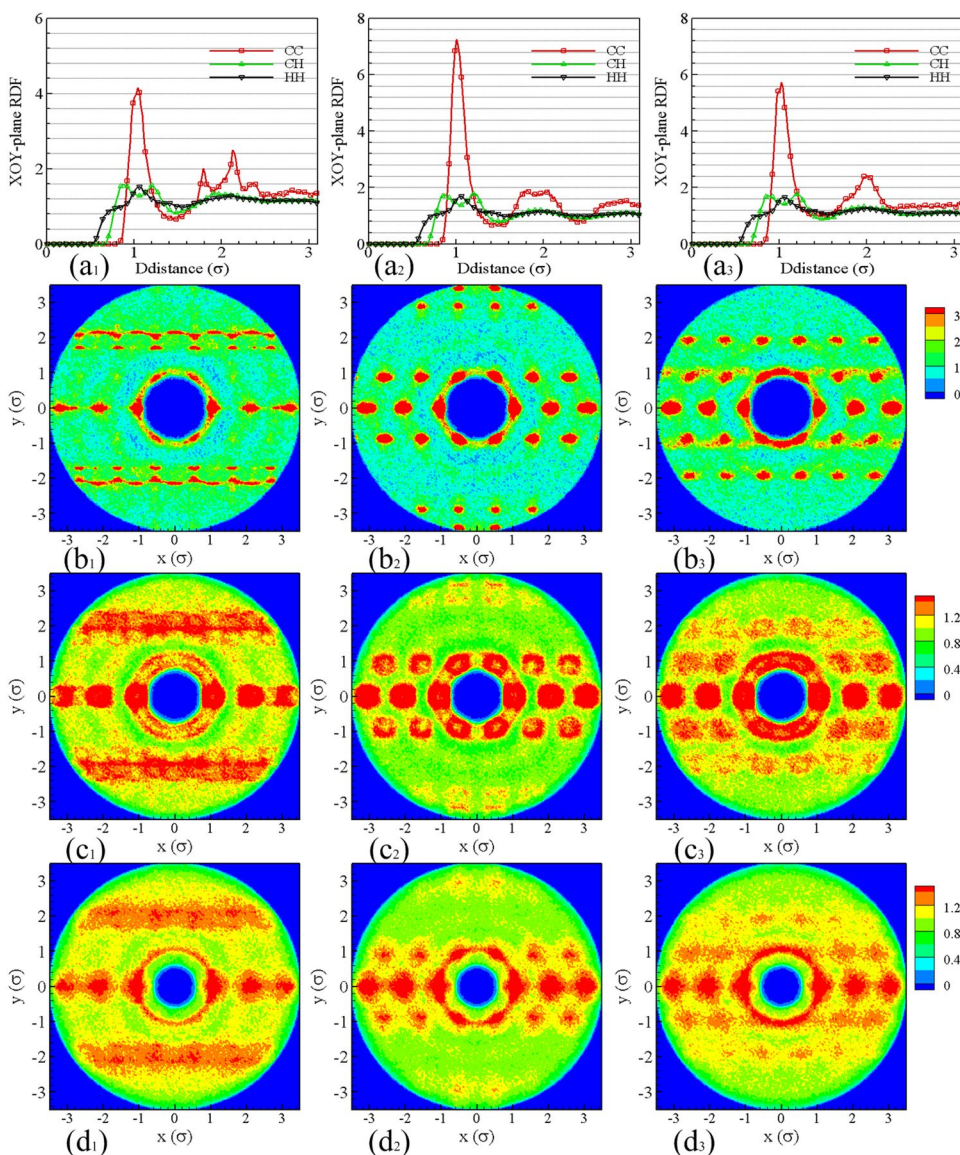
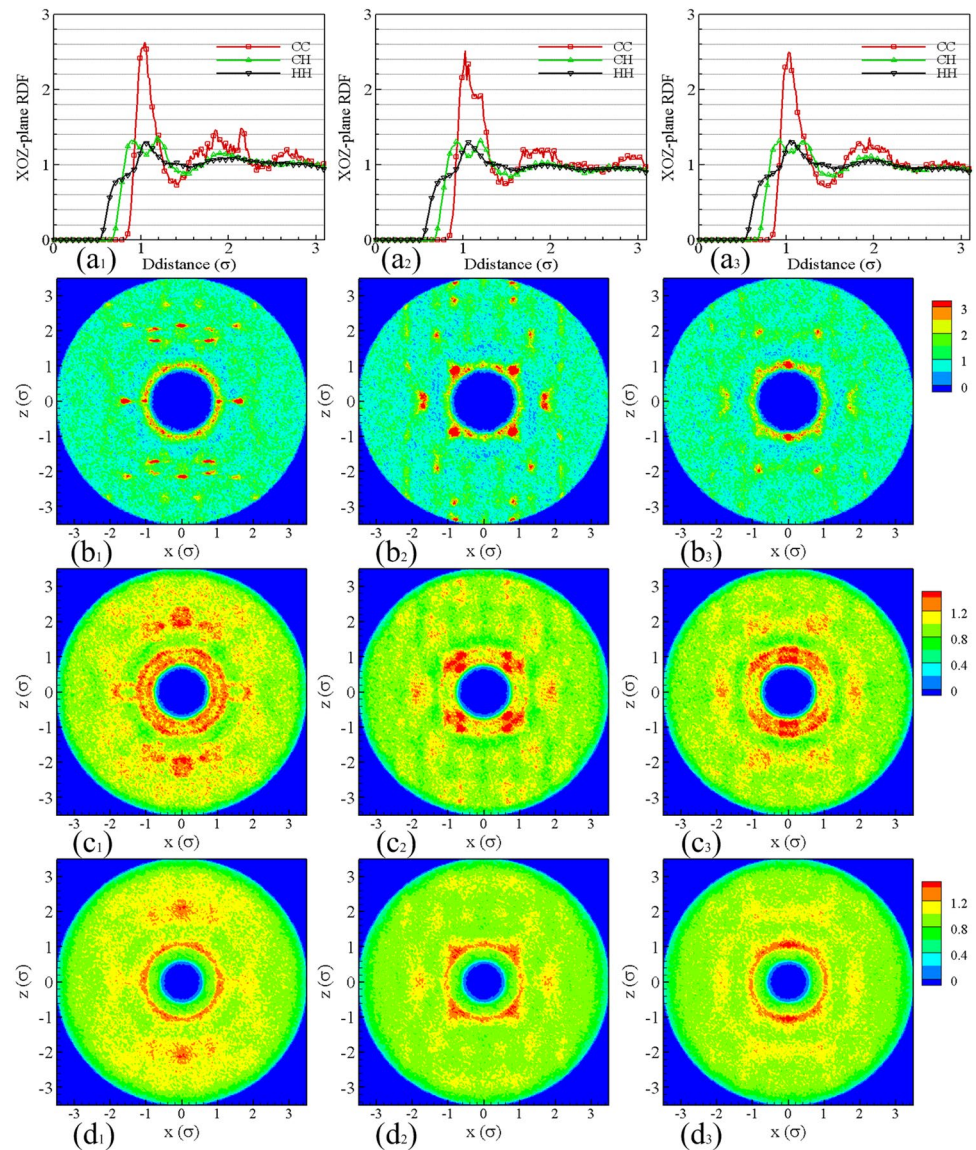


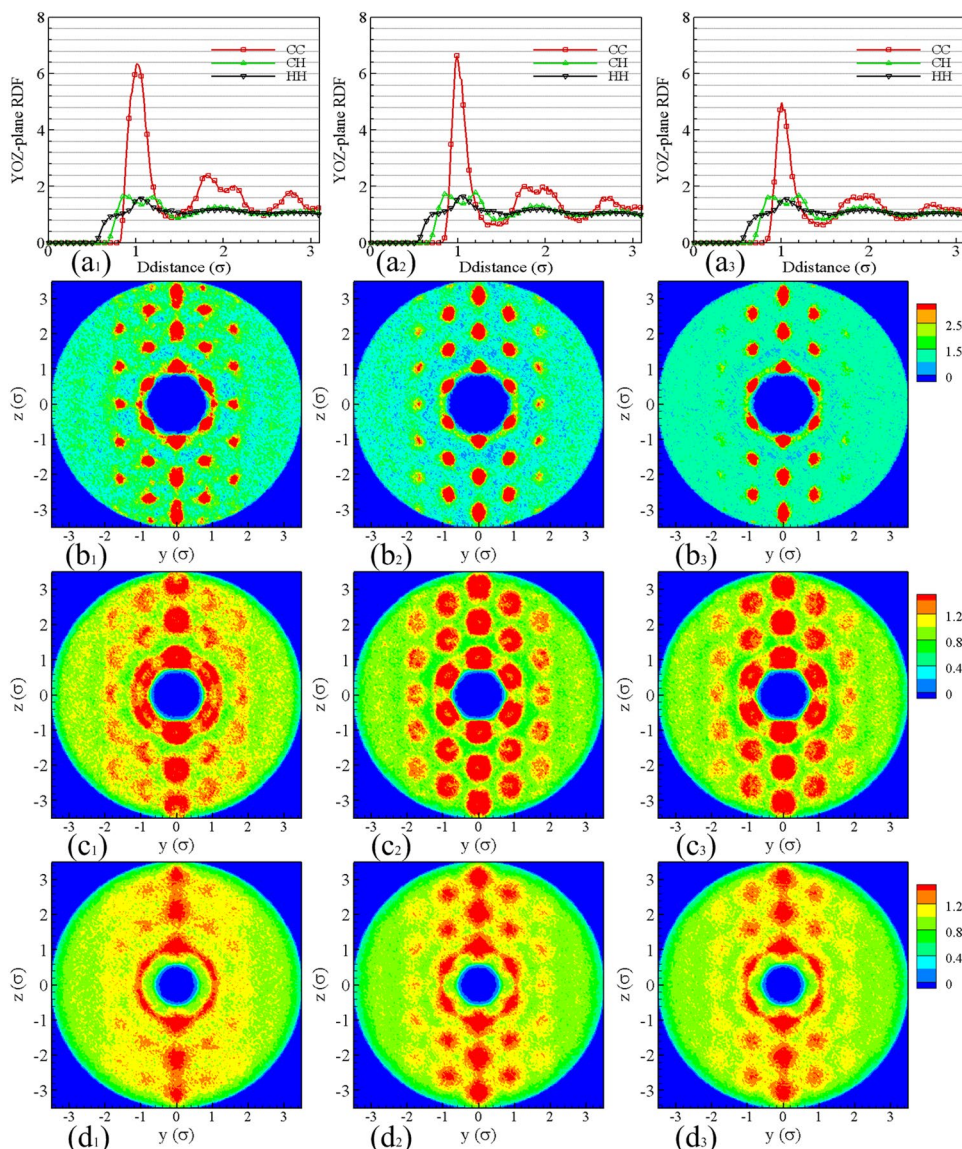
Fig. 6 **a**₁–**a**₃ Total average projections of the radial distribution function [$g_{CC}(r)$, $g_{CH}(r)$ and $g_{HH}(r)$] plotted over the whole channel region in XOZ plane with different roughness. The contours of radial distribution function [$g_{CC}(r)$, $g_{CH}(r)$ and $g_{HH}(r)$] projected onto XOZ plane for [**b**₁–**b**₃: $g_{CC}(r)$, **c**₁–**c**₃: $g_{CH}(r)$ and **d**₁–**d**₃: $g_{HH}(r)$] plotted for different periodic roughness of nanochannel walls



pair distribution functions [$g_{CC}(r)$ (Fig. 5b₁–b₃), $g_{CH}(r)$ (Fig. 5c₁–c₃) and $g_{HH}(r)$ (Fig. 5d₁–d₃)] presents ribbon pattern in x-direction (streaming direction). We also observe that $g_{CC}(r)$, $g_{CH}(r)$ and $g_{HH}(r)$ have more obvious diversity from the contour (Fig. 5b₁–b₃, c₁–c₃ and d₁–d₃) than curve (Fig. 5a₁–a₃). And note in the plot for different rough wavelengths that traces of the next-nearest neighbor peak remain as “islands” of elevated pair probability rather than a continuous ring. This behavior is attributed to the solid wall boundary condition and the statistical averaging. As a matter of fact, these numerical results show that the roughness solid wall boundary has a major influence on the microstructure properties if we observe them from z-direction. Considering XOZ plane, the first peak values of the projection of C-atom radial distribution functions (red lines in Fig. 6a₁–a₃) do not almost depend on the roughness, but the curve form has obvious differences. These diversities can be clearly seen

from Fig. 6b₁–b₃. Meantime, Fig. 6c₁–c₃ and d₁–d₃ plots the projection radial distribution functions for $g_{CH}(r)$ and $g_{HH}(r)$, whose local peak values have significant diversity from y-direction observation. We attribute it to the atom interaction force in z axis orientation and the streaming. Figure 7 plots the projected radial distribution function on YOZ plane. The first peak values of C-atom radial distribution function (Fig. 7a₁–a₃) reduce tendency when the wavelength is larger than $\lambda_2 = 4.31 \sigma$. The contour of atom pair distribution functions [$g_{CC}(r)$ (Fig. 7b₁–b₃), $g_{CH}(r)$ (Fig. 7c₁–c₃) and $g_{HH}(r)$ (Fig. 7d₁–d₃)] presents ribbon pattern in y-direction. And the number of ribbon decreases with the increasing wavelength. Besides, we notice that the anisotropy microstructure of methane nanofluidic displays complex variations from Figs. 5, 6, and 7. And the values of RDFs do not converge to 1 at 3σ . These reasons can be attributed to the different atom interaction force and boundary conditions

Fig. 7 **a₁–a₃** Total average projections of the radial distribution function [$g_{CC}(r)$, $g_{CH}(r)$ and $g_{HH}(r)$] plotted over the whole channel region in YOZ plane with different roughness. The contours of radial distribution function [$g_{CC}(r)$, $g_{CH}(r)$ and $g_{HH}(r)$] projected onto YOZ plane for [**b₁–b₃**: $g_{CC}(r)$, **c₁–c₃**: $g_{CH}(r)$ and **d₁–d₃**: $g_{HH}(r)$] plotted for different periodic roughness of nanochannel walls



in three directions. The similar results can be found in the literature (Sofos et al. 2015). All numerical results show that the roughness of nanochannel wall has a remarkable influence on the microstructure properties of methane nanofluidic. We consider the reason to the complex atom force of interaction (fluid atom and wall atom) and shear force due to the streaming.

3.2 Fluid–wall interaction strength

To further investigate the impacts of fluid molecule and wall atom interaction force on the microstructure properties and system dynamics of methane nanofluidic, three fluid–wall interaction strength factors ($\chi_1 = 0.5$, $\chi_2 = 1.0$, $\chi_3 = 1.5$) are employed in this section at the given roughness ($2A = \lambda_1 = 2.15 \sigma$) of nanochannel wall. The total average number density distribution profiles of C and H atoms

are displayed in Fig. 8. In the middle of the nanochannel regions, the atom number densities are that more or less constant density of bulk system is reached. The atom (C and H) number density increases with the increasing fluid–wall interaction strength factor. Inside the cavities, all peak values of atoms (C and H) number density are obviously decreased with the increasing fluid–wall strength factor. Moreover, all peak values of C-atom number density are bigger than those of H atom, and the valley width of H atom number density is lower than that of C atom. The minimum values of the atoms (C and H) number density distributions are almost the same for all strength factors. Near the rough wall regions, we observe that the peak positions of C-atom number density distributions are just that of valley, which indicates the space structure characteristic of methane molecule (tetrahedra). The numerical results show that the fluid–wall interaction strength factor has a marked impact on C (H) atom number

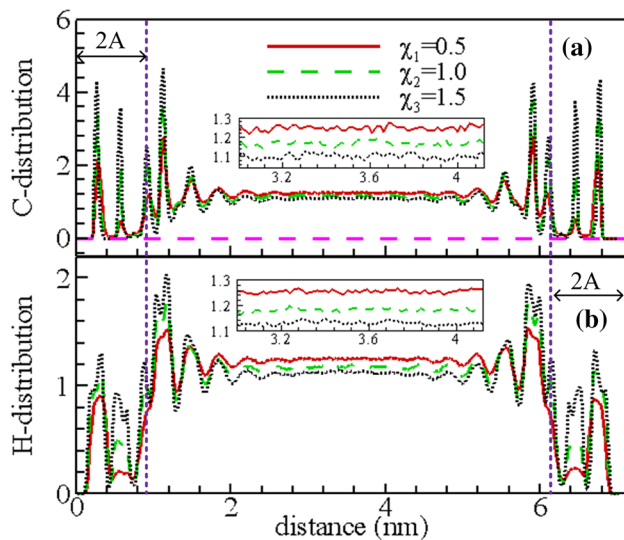


Fig. 8 Total average C-distribution and H-distribution profiles plotted for different fluid–wall interaction strength over the whole channel region

density distribution. Because of the strong layering of fluid atoms near the nanochannel walls, methane fluids are inhomogeneous. Besides, the anisotropy of methane molecule increases with the values of fluid–wall interaction strength factor increase near nanochannel wall. It may be attributed to the fact that the translational mobility or rotary movement of methane becomes slow near nanochannel walls and inside cavity (Jiang et al. 2017c). The results are similar to those of Sofos et al. for liquid argon through krypton nanochannel (Sofos et al. 2010, 2012, 2016) or Duan et al. for polymer melts in atomically flat nanochannel (Duan et al. 2015). It indicates that the fluid atom localization inside the cavities increases while the fluid–wall interaction strength factor

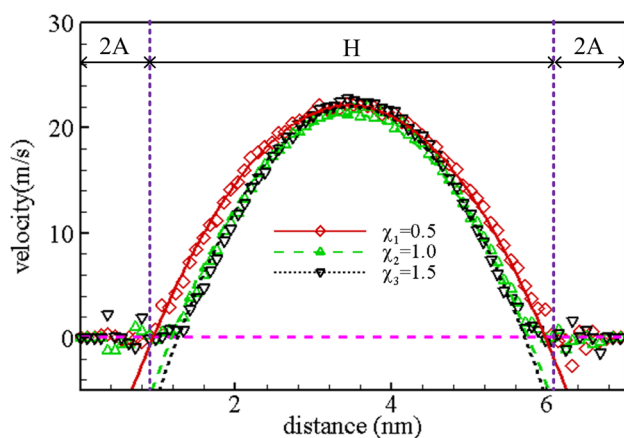


Fig. 9 Total average streaming velocity profiles plotted for different fluid–wall interaction strength over the whole channel region

increases, i.e., the strength of fluid–wall interaction has a major influence on the fluid atom localization distribution.

We present the total average streaming velocity profiles for different fluid–wall interaction strength in Fig. 9. The solid (velocity profile) was obtained by fitting 260 simple points in the middle of the nanochannel. The maximum values of velocity have slight diversity, indicating that the effect of fluid–wall interaction strength on the maximum values of velocity is not significant. However, the opening width of velocity profile increases with the decreasing fluid–wall interaction strength factor. And this change is diminished gradually as $\chi \geq 1.0$. This may be due to the fact that the methane molecules suffered interaction force increases when it is close to the roughness nanochannel walls. These numerical results show that the fluid–wall interaction strength has a significant influence on the system dynamic of methane nanofluidic moving the rough nanochannel surfaces.

The diversity of average velocity for fluid molecule impacts on the diffusivity of methane nanofluidic in rough nanochannel. To study the diffusivity of methane nanofluidic, firstly, we give the normalized velocity autocorrelation functions (obtained three different fluid–wall interaction strength factors at a given roughness) displayed in Fig. 10, showing all the normalized velocity autocorrelation functions approximate to zero at about $t = 1.2$ ps. And the time (normalized velocity autocorrelation functions value approximates to zero) decreases with the increasing fluid–wall interaction strength factor. The minimum value of normalized velocity autocorrelation function increases with the increasing fluid–wall interaction strength factor at the same oscillation period, and the peak values present opposite conclusion. Moreover, inside rough cavities, the fluid molecule interaction force and residence time depend on the fluid–wall interaction strength. Besides, we can see from Fig. 10 that the oscillations frequency of normalized velocity autocorrelation functions increases when the fluid–wall interaction strength factor increases. We attributed it to the trajectories of molecules obtained from molecule force at different fluid–wall interaction strengths for the disparity in the normalized velocity autocorrelation function. In fact,

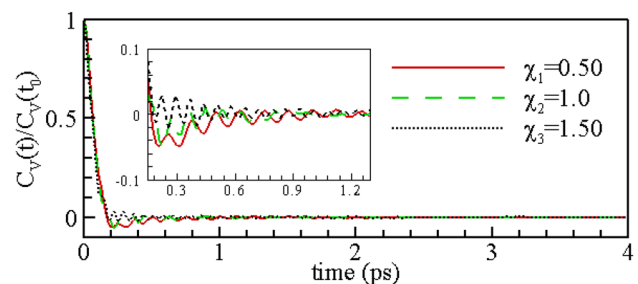


Fig. 10 The normalized velocity autocorrelation function plotted for different fluid–wall interaction strength over the whole channel region

the diffusion coefficient, being proportional to single particle correlations in pure fluids, is the transport coefficient value most reliably obtained from the molecular trajectories. The corresponding diffusion coefficient values are given as $70.34 \pm 0.89 (10^{-10} \text{ m}^2 \text{ s}^{-1})$, $71.11 \pm 1.07 (10^{-10} \text{ m}^2 \text{ s}^{-1})$ and $73.41 \pm 0.82 (10^{-10} \text{ m}^2 \text{ s}^{-1})$ for $\chi_1 = 0.5$, $\chi_2 = 1.0$ and $\chi_3 = 1.5$, respectively. The diffusion coefficient values increases with increasing the fluid–wall interaction strength, indicating that the fluid–wall interaction strength plays a significant role in the diffusivity of methane nanoflow through rough nanochannel walls.

Figures 11, 12, and 13 show the curve and contour of the radial distribution functions [$g_{CC}(r)$, $g_{CH}(r)$ and $g_{HH}(r)$] projection on three planes (XOY, XOZ and YOZ) for three fluid–wall interaction strength factors in the whole nanochannel. In XOY plane, it can be seen from Fig. 11a₁–a₃ that the first peak value of C-atom radial distribution

function increases as the fluid–wall interaction strength factor increases. And the other peak values present various variations. The diversities of C-atom radial distribution function contour projected on XOY plane are also shown in Fig. 11b₁–b₃. Obviously, these present results show a greater level of detail than the curve (Fig. 11a₁–a₃) at the same conditions. Moreover, the red island regions increase with the increasing fluid–wall interaction strength factor. Figure 11c₁–c₃ and d₁–d₃ displays the change of the $g_{CH}(r)$ and $g_{HH}(r)$ project on XOY plane when the fluid–wall interaction strength factor increases, respectively. These behaviors are attributed to the fluid atom force suffered from the wall atom and streaming in x-direction. In Fig. 12, all projected radial distribution functions present various difference on XOZ plane. More precisely, the first peak values of $g_{CC}(r)$ (from Fig. 12a₁–a₃) decrease with the increasing the fluid–wall interaction strength factor.

Fig. 11 a₁–a₃ Total average projections of the radial distribution function [$g_{CC}(r)$, $g_{CH}(r)$ and $g_{HH}(r)$] plotted over the whole channel region in XOY plane with different fluid–wall interaction strength. The contours of radial distribution function [$g_{CC}(r)$, $g_{CH}(r)$ and $g_{HH}(r)$] projected onto XOY plane for [b₁–b₃: $g_{CC}(r)$, c₁–c₃: $g_{CH}(r)$ and d₁–d₃: $g_{HH}(r)$] plotted for different fluid–wall interaction strength

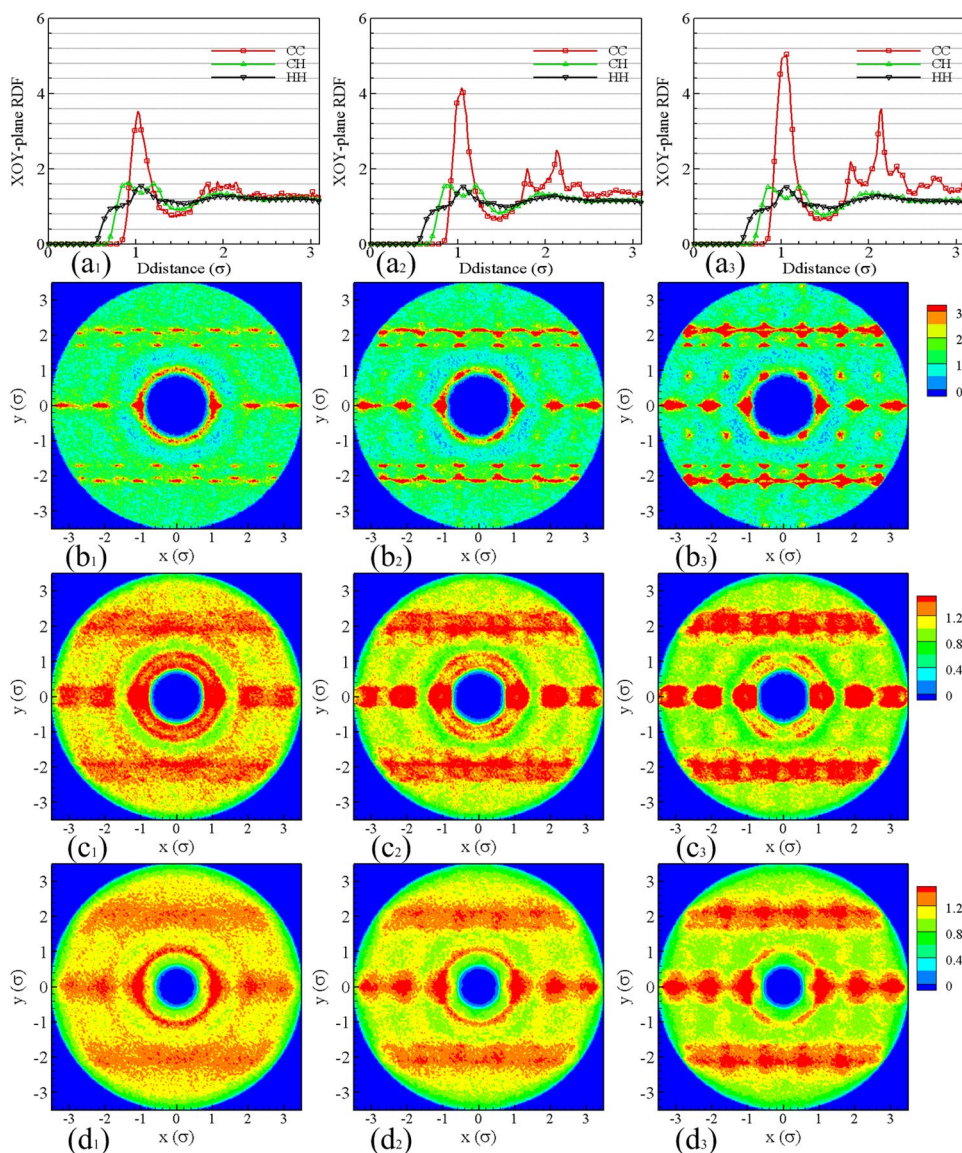
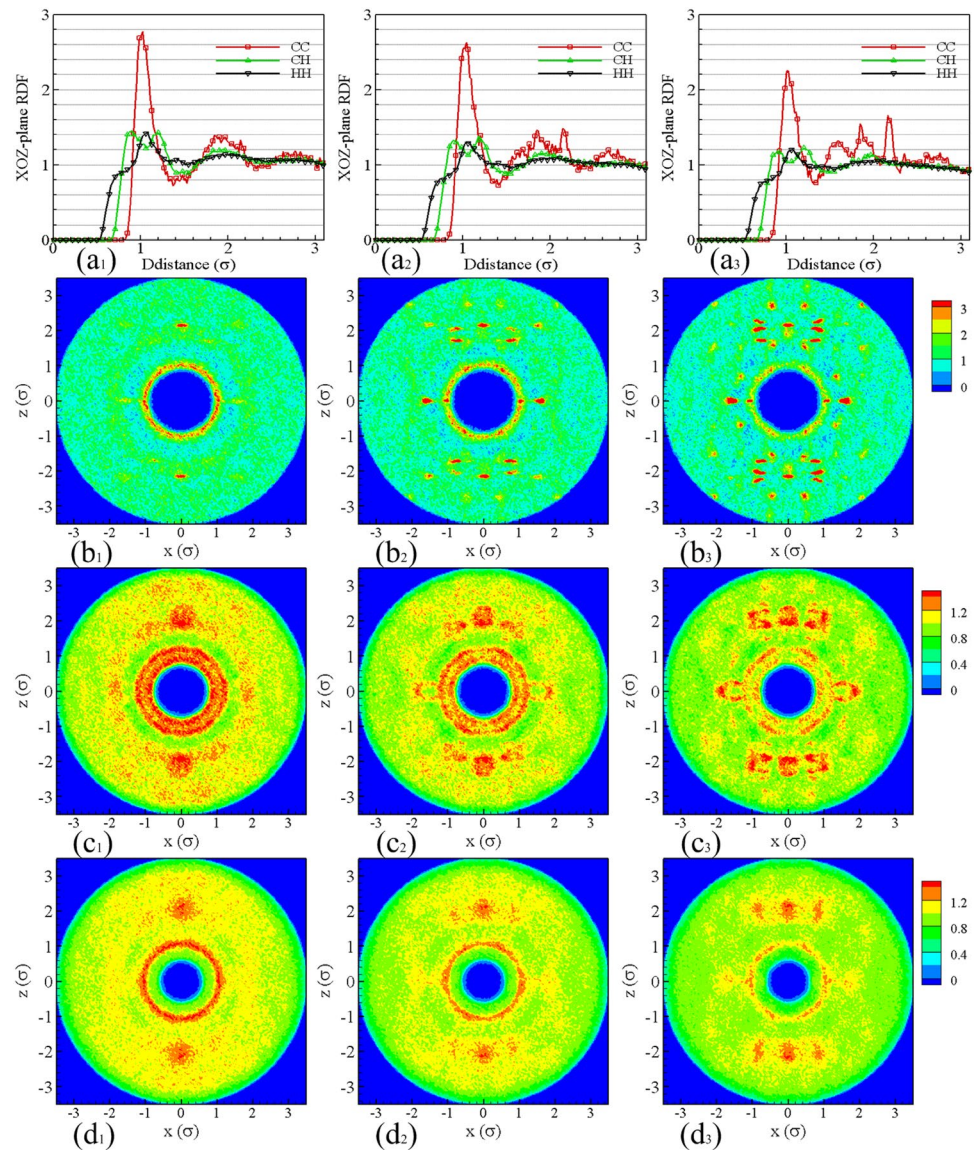


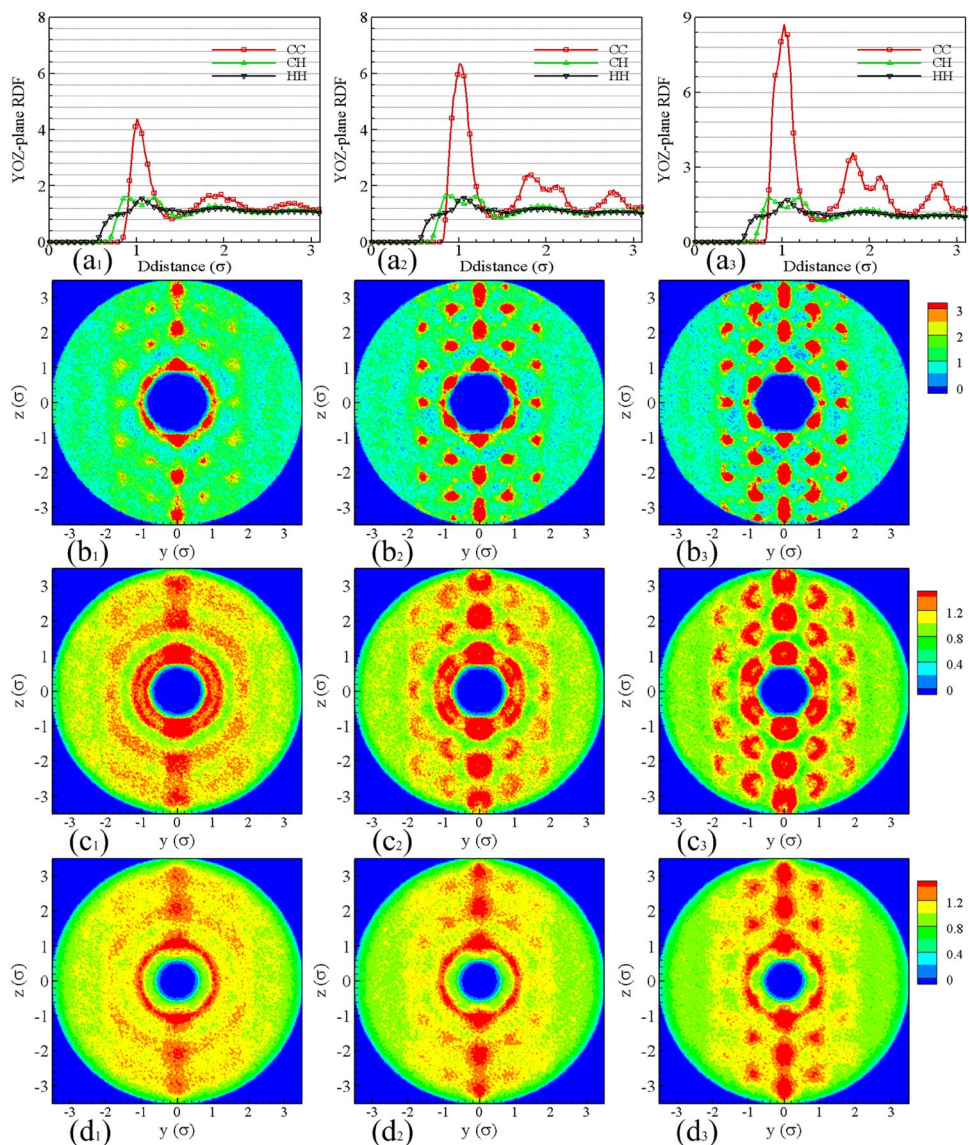
Fig. 12 **a₁–a₃** Total average projections of the radial distribution function [$g_{CC}(r)$, $g_{CH}(r)$ and $g_{HH}(r)$] plotted over the whole channel region in XOZ plane with different fluid–wall interaction strength. The contours of radial distribution function [$g_{CC}(r)$, $g_{CH}(r)$ and $g_{HH}(r)$] projected onto XOZ plane for [**b₁–b₃**: $g_{CC}(r)$, **c₁–c₃**: $g_{CH}(r)$ and **d₁–d₃**: $g_{HH}(r)$] plotted for different fluid–wall interaction strength



Meantime, the number of peak value increases when the fluid–wall interaction strength factor increases. This feature is clearly shown in Fig. 12b₁–b₃ by the contours, which describes the change of radial distribution functions peak value. Although the projected radial distribution curves ($g_{CH}(r)$ and $g_{HH}(r)$) are not obviously different in Fig. 12a₁–a₃, the contour displays the difference for $g_{CH}(r)$ and $g_{HH}(r)$. We attribute the behavior to the fluid atom force suffered from the solid wall boundary and space fluid molecule model. Figure 13 gives the projected radial distribution functions [$g_{CC}(r)$, $g_{CH}(r)$ and $g_{HH}(r)$] on the YOZ plane. The number of $g_{CC}(r)$ (Fig. 13a₁–a₃) decreases as the fluid–wall interaction strength increases. And the peak values [$g_{CC}(r)$] visibly present the rising tendency. The contours are plotted in Fig. 13b₁–b₃, which also shows the results from the space distribution. Figure 13c₁–c₃

and d₁–d₃ plots the distributions of the projected radial functions $g_{CH}(r)$ and $g_{HH}(r)$, respectively. Clearly, in the plot for different fluid–wall interaction strength factors that traces of the elevated pair probability peak remain as “islands” rather than a continuous ring. And the region of deep color islands increases with the increasing fluid–wall interaction strength. Besides, the contours also display the remarkable change of projected radial distribution function on three planes, which denote that the anisotropy of methane poiseuille flow increases when the fluid–wall interaction strength increases. These results indicate that the fluid–wall interaction strength has a significant influence on the microstructure of methane poiseuille flow in rough nanochannel walls.

Fig. 13 **a₁–a₃** Total average projections of the radial distribution function [$g_{CC}(r)$, $g_{CH}(r)$ and $g_{HH}(r)$] plotted over the whole channel region in YOZ plane with different fluid–wall interaction strength. The contours of radial distribution function [$g_{CC}(r)$, $g_{CH}(r)$ and $g_{HH}(r)$] projected onto YOZ plane [**b₁–b₃**: $g_{CC}(r)$, **c₁–c₃**: $g_{CH}(r)$ and **d₁–d₃**: $g_{HH}(r)$] plotted for different fluid–wall interaction strength



3.3 Body driving force

The body driving force has a major effect on the properties of nanofluidic (Karniadakis et al. 2006), because the large body driving force results in the compressibility effects of fluid flow of the nanochannel. To avoid compressibility effects, the Mach number should be less than 0.33 (Ranjith et al. 2013). The relevant research of methane nanofluidic can be seen in our previous work (Jiang et al. 2016b). In this study, to investigate the impacts of body-driving force on the microstructure and system dynamics of methane nanofluidic, four body driving forces ($f = \{0.05 \epsilon/\sigma, 0.075 \epsilon/\sigma, 0.10 \epsilon/\sigma, 0.125 \epsilon/\sigma\}$) are selected in this subsection at given roughness of nanochannel wall and fluid–wall interaction strength. The total average atom (C and H) number density distribution profiles is plotted in Fig. 14. In the middle of the nanochannel regions,

the atom average number density presents a rising tendency for the above four body driving forces; the H atom average number density is a trend of steady and then increases with body driving force; and the C-atom average number density has no obvious change as the H atom. The reason could be attribute to the space structure of methane molecule model or the increase in the Mach number. Inside the cavities, all peak values of atoms (C and H) number density are slightly decreased as body driving force decreases. Moreover, all peak values of C-atom number density are bigger than that of H atom, and the valley width of H atom number density is lower than that of C atom. Moreover, the minimum values of the atoms (C and H) number density distributions are almost the same in this simulation. Near the rough wall regions, we observe that the peak positions of C-atom number density distributions are just the valley site because of the space structure characteristic of methane molecule (tetrahedra).

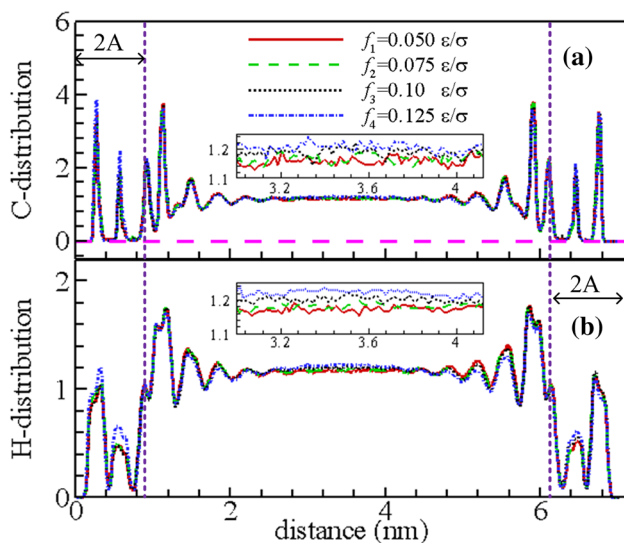


Fig. 14 Total average C-distribution and H-distribution profiles plotted for different body driving forces over the whole channel region

The present numerical results denote that the body driving force has an impact on C (H) atom number density distribution. In addition, the anisotropy of methane molecule increases when the values of body driving force increase near nanochannel wall. It may be attributed to the fact that the translational mobility or rotary movement of methane becomes slow near nanochannel wall and inside cavity. The results are similar to those of Sofos et al. for liquid argon through krypton nanochannel (Liakopoulos et al. 2016). It indicates that the fluid atom localization inside the cavities increases while the body driving force increases. i.e., the body driving force has a major influence on the fluid atom localization distribution.

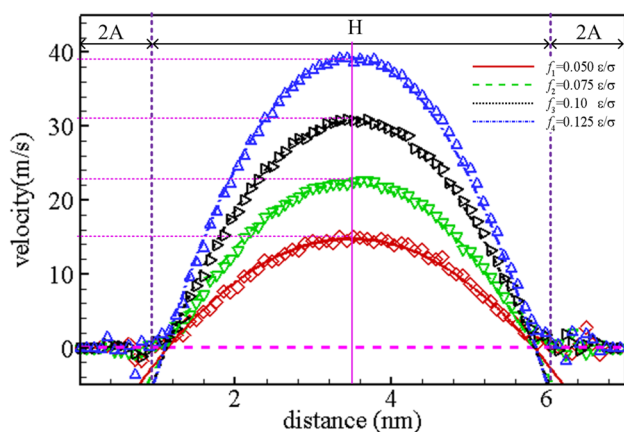


Fig. 15 Total average streaming velocity profiles plotted for different body driving forces over the whole channel region

The total average streaming velocity profiles for different body driving forces are presented in Fig. 15. We observe that the effective means of facilitating fluid flow in rough nanochannel are body driving force. The streaming velocity change approximates linear regime as the body force $f_x \leq 0.125$. Moreover, it can be seen from Fig. 15 that a larger body driving force produces a higher velocity profile distribution. These results are similar to those published regarding liquid argon (Liakopoulos et al. 2016). These numerical results show that the body driving force has a significant impact on the velocity distribution of methane nanofluidic flowing rough nanochannel.

In Fig. 16, the normalized velocity autocorrelation functions are plotted for different body driving forces at a given roughness ($\lambda_2 = 2A = 2.15 \sigma$) and fluid–wall interaction strength ($\chi_2 = 1.0 \epsilon/\sigma$). It can be seen from Fig. 16 that the normalized velocity autocorrelation functions arrive at zero about $t = 1.0$ ps. And the time (normalized velocity autocorrelation functions value approximates to zero) slightly decreases with the increasing body driving force. The minimum value of normalized velocity autocorrelation function decreases as body driving force decreases, and the peak values present opposite conclusion. These results can be explained by nature of molecule moving track depending on driving force and fluid–wall interaction force in x -direction. Moreover, the oscillating period of normalized velocity autocorrelation function is not changed for all body driving force, which indicates that the molecules have the same time of back and forth movement inside the cavities, because of the body driving force in x -direction (it does not help the molecule escaping the confined by cavities). We attribute to the trajectories of molecules obtained from molecule force at different body driving forces for the disparity in the normalized velocity autocorrelation function. In fact, the diffusion coefficient, being proportional to single particle correlations in pure fluids, is the transport coefficient which is most reliably calculated by the molecular trajectories. The calculated diffusion coefficient values for four body driving forces are shown as follows 71.33 ± 0.76 ($10^{-10} \text{ m}^2 \text{ s}^{-1}$), 71.05 ± 1.37 ($10^{-10} \text{ m}^2 \text{ s}^{-1}$), 72.12 ± 0.64 ($10^{-10} \text{ m}^2 \text{ s}^{-1}$)

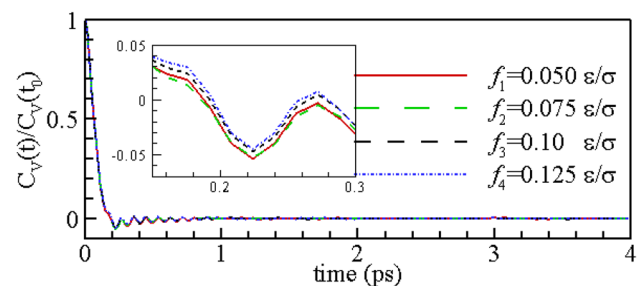


Fig. 16 The velocity autocorrelation function plotted for body driving force over the whole channel region

and $72.89 \pm 0.82 (10^{-10} \text{ m}^2 \text{ s}^{-1})$. The slight difference can be attributed to the statistical calculation error and the atom numerical density distribution. The calculation result indicates that the body driving force has no obvious influence on the diffusivity of methane nanoflow in rough nanochannel at given other initial conditions. It is similar to the results of liquid argon for Poiseuille flow in a system confined by krypton nanochannel wall (Sofos et al. 2009a, b).

The curve and contour plots within three planes (XOY, XOZ and YOZ) providing quantitative information on the distortion of the radial distribution functions $[g_{CC}(r), g_{CH}(r)$ and $g_{HH}(r)]$ under different body driving forces for methane nanoflows are presented in Figs. 17, 18, 19. It can be seen from Figs. 17, 18, 19 that the curve and contour of projections radial distribution function $[g_{CC}(r), g_{CH}(r)$ and $g_{HH}(r)]$ have tiny difference, which can be considered

as thermoacoustic oscillation or calculation errors. These present results indicate that the body driving force has no significant impact on the microstructure of methane Poiseuille flow in nanochannel at given projections plane. This reason is that methane fluid could be attributed to simple fluid. Since the body driving force mainly determines the shear stress of fluid, the microstructure of simple fluid was not enslaved to shear stress (Morris 2009). And the diversities of microstructure are shown in Figs. 17, 18, and 19 on different planes, clearly illustrating the anisotropy of microstructure for methane nanofluidic moving the nanochannel at given simulation condition. These simulation results indicate that the body driving force has no remarkable influence on the anisotropy characteristic of methane Poiseuille flow.

Fig. 17 **a₁–a₃** Total average projections of the radial distribution function $[g_{CC}(r), g_{CH}(r)$ and $g_{HH}(r)]$ plotted over the whole channel region in XOY plane with different body driving force. The contours of radial distribution function $[g_{CC}(r), g_{CH}(r)$ and $g_{HH}(r)]$ projected onto XOY plane [**b₁–b₃**: $g_{CC}(r)$, **c₁–c₃**: $g_{CH}(r)$ and **d₁–d₃**: $g_{HH}(r)$] plotted for different body driving forces

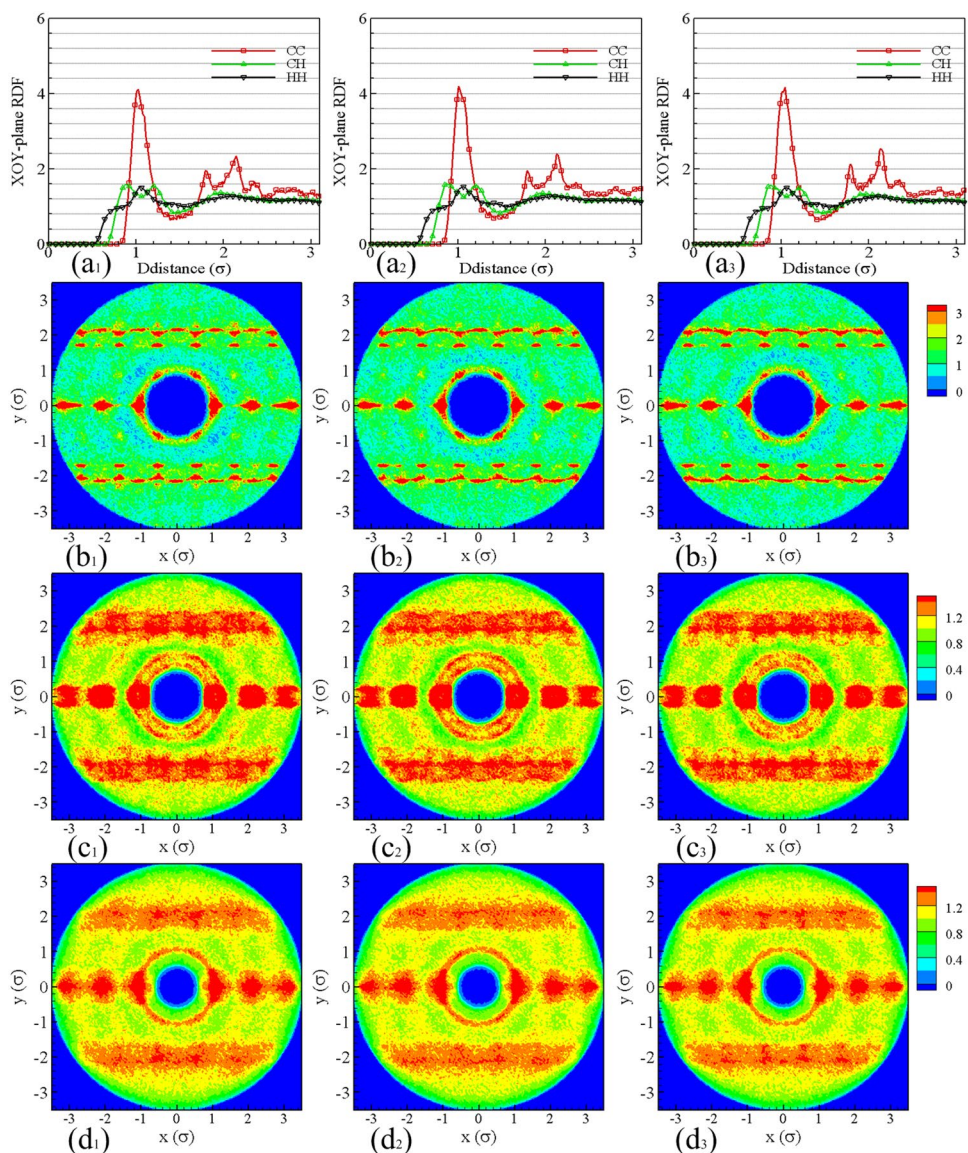
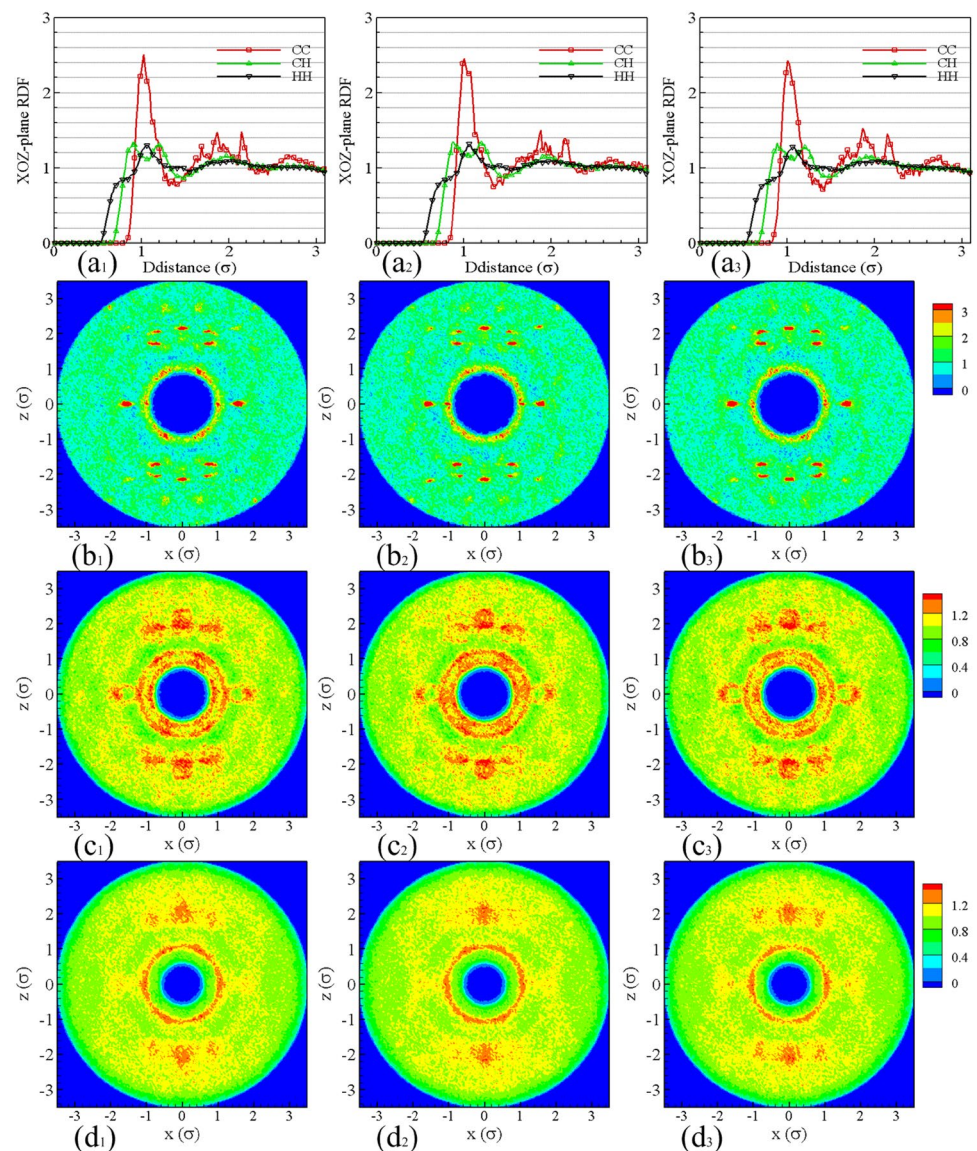


Fig. 18 **a₁–a₃** Total average projections of the radial distribution function [$g_{CC}(r)$, $g_{CH}(r)$ and $g_{HH}(r)$] plotted over the whole channel region in XOZ plane with different body driving forces. The contours of radial distribution function [$g_{CC}(r)$, $g_{CH}(r)$ and $g_{HH}(r)$] projected onto XOZ plane [**b₁–b₃**: $g_{CC}(r)$, **c₁–c₃**: $g_{CH}(r)$ and **d₁–d₃**: $g_{HH}(r)$] plotted for different body driving forces



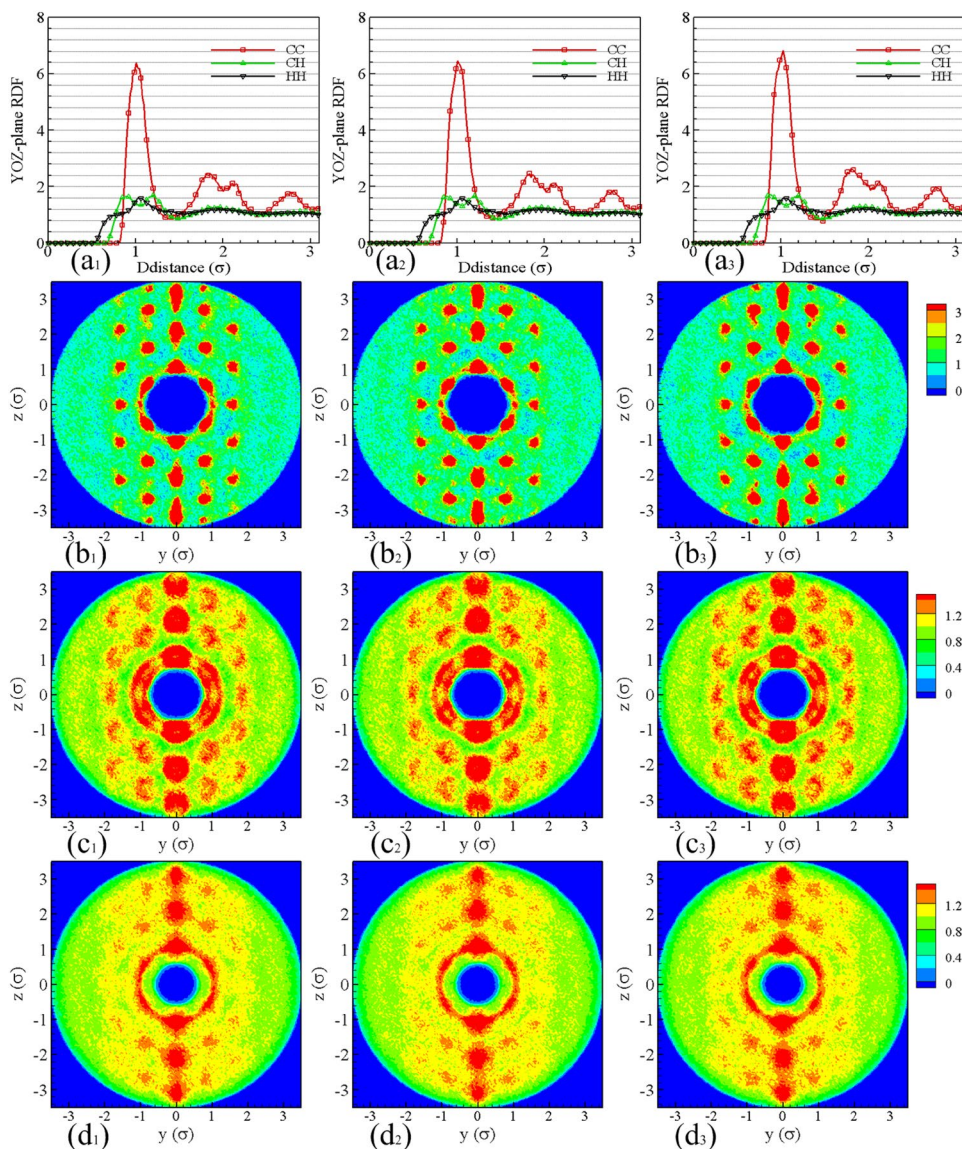
3.4 Cutoff radius

In nanoscale, the force of molecules interaction plays a crucial role in NEMSMD simulation. The system properties are directly determined by force of intermolecular interaction, which is manipulated by the molecule model, cutoff radius and other factors. The cutoff radius, among many factors, is considered to be directly associated with the simulation times and the validity of simulation results at a given molecule model. In this subsection, thus, we study the effect of cutoff radius on the microstructure information and system dynamics of methane nanofluidic. To study the influence of cutoff radius on the microstructure and system dynamics of methane nanofluidic, the four cutoff radii ($r_{\text{cut}} = \{1.0 \sigma, 2.0 \sigma, 2.5 \sigma, 3.0 \sigma\}$, for $r_{\text{cut}} = 2.5 \sigma$, the simulation results can be seen from 3.3 Section) are employed in this subsection at the given roughness of

nanochannel wall ($\lambda = 2.15 \sigma$, $2A = 2.15 \sigma$) and fluid–wall interaction strength factor ($\chi = 1.0$).

Figure 20 presents the total average atom (C and H) number density distribution profiles. It can be seen from Fig. 20 that the atom average number density presents a decreasing tendency with cutoff radius in the middle of the nanochannel regions, and the H atom average number density has a more significant decreasing tendency than that of C atom when the cutoff radius increases. This is due to the space structure of methane molecule model. For $r_{\text{cut}} = 1.0 \sigma$, the first peak values of atoms (C and H) number density are obviously bigger than those of other cutoff radii inside the cavities. Moreover, when $r_{\text{cut}} \geq 2.0 \sigma$, all peak values of C and H atom number density increase with the increasing cutoff radius, and the valley values are nearly the same. Near the rough wall regions, we observe that the peak values of C and H atoms number density distributions increase when cutoff

Fig. 19 **a₁–a₃** Total average projections of the radial distribution function [$g_{CC}(r)$, $g_{CH}(r)$ and $g_{HH}(r)$] plotted over the whole channel region in YOZ plane with different body driving forces. The contours of radial distribution function [$g_{CC}(r)$, $g_{CH}(r)$ and $g_{HH}(r)$] projected onto YOZ plane [**b₁–b₃**; $g_{CC}(r)$, **c₁–c₃**; $g_{CH}(r)$ and **d₁–d₃**; $g_{HH}(r)$] plotted for different body driving forces



radius increases. And the difference in the peak values is almost the same when $r_{cut} \geq 2.0 \sigma$, which indicates that the intermolecular interactions force is not a significant variation from other fluid molecules and wall. Besides, the anisotropy of methane molecule increases with the values of cutoff radius at near nanochannel wall. One could attribute it to the difference of intermolecular interactions force obtained from fluid molecules or wall atoms. It denotes that it is vital to select a proper cutoff radius for NEMSMD simulations.

We show the velocity profiles for different cutoff radii in Fig. 21. A significant difference between $r_{cut} = 1.0 \sigma$ and $r_{cut} \geq 2.0 \sigma$ velocity profile is the existence of maximum values in the rough nanochannel. Although the maximum value of velocity profile is slightly different obtained between $r_{cut} = 2.0 \sigma$ and $r_{cut} = 3.0 \sigma$, the diversity is rather small, and can be ignored if the calculated times are considered. In this simulation, the calculation time is about 82,956

s for $r_{cut} = 3.0 \sigma$, (69,533 s for $r_{cut} = 2.5 \sigma$), which is larger than that 61,202 s for $r_{cut} = 2.0 \sigma$, since the interaction pairs rapidly increase with increasing cutoff radius. Thus, this result suggests that the cutoff radius $r_{cut} \geq 2.0 \sigma$ can be selected for studying the methane nanofluidic by using NEMSMD simulations.

Figure 22 shows the normalized velocity autocorrelation functions, which are close to zero at about $t = 1.5$ ps. And the time (normalized velocity autocorrelation functions value approximates to zero) decreases with the increasing cutoff radius. The first minimum values of normalized velocity autocorrelation function present various variations. This is because of the complex interactions of the methane molecules near the walls [specially speaking, the methane molecule obtain the interaction force from the other methane molecules via $U(r_{ij})$ and wall atoms by $U_{FW}(r_{ij})$ as it is close to the walls ($\leq r_{cut}$)]. And the periodic phenomena

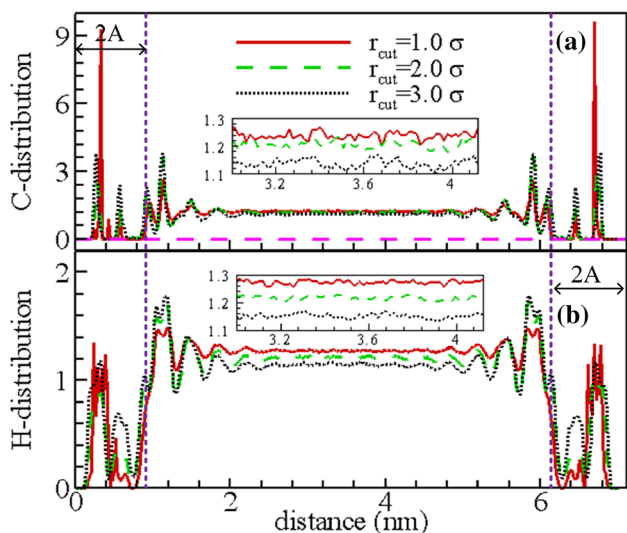


Fig. 20 Total average C-distribution and H-distribution profiles plotted for different cutoff radii over the whole channel region

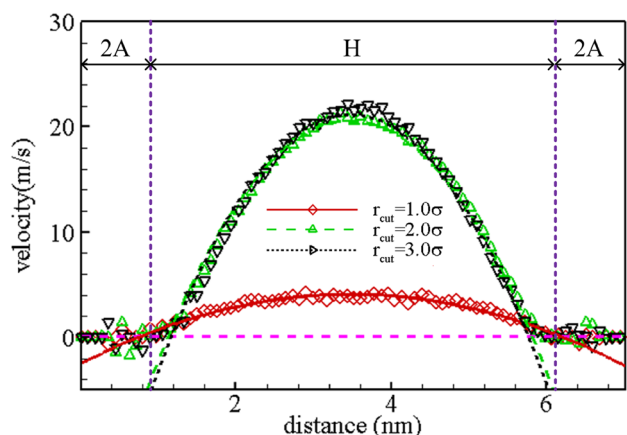


Fig. 21 Total average streaming velocity profiles plotted for different cutoff radii over the whole channel region

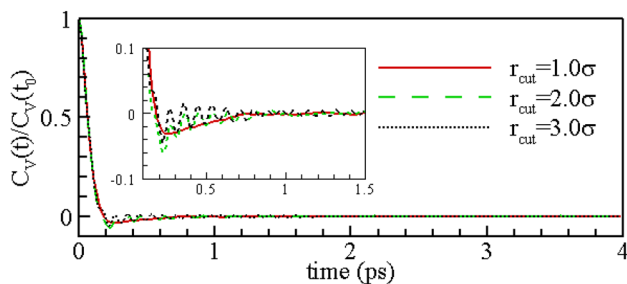
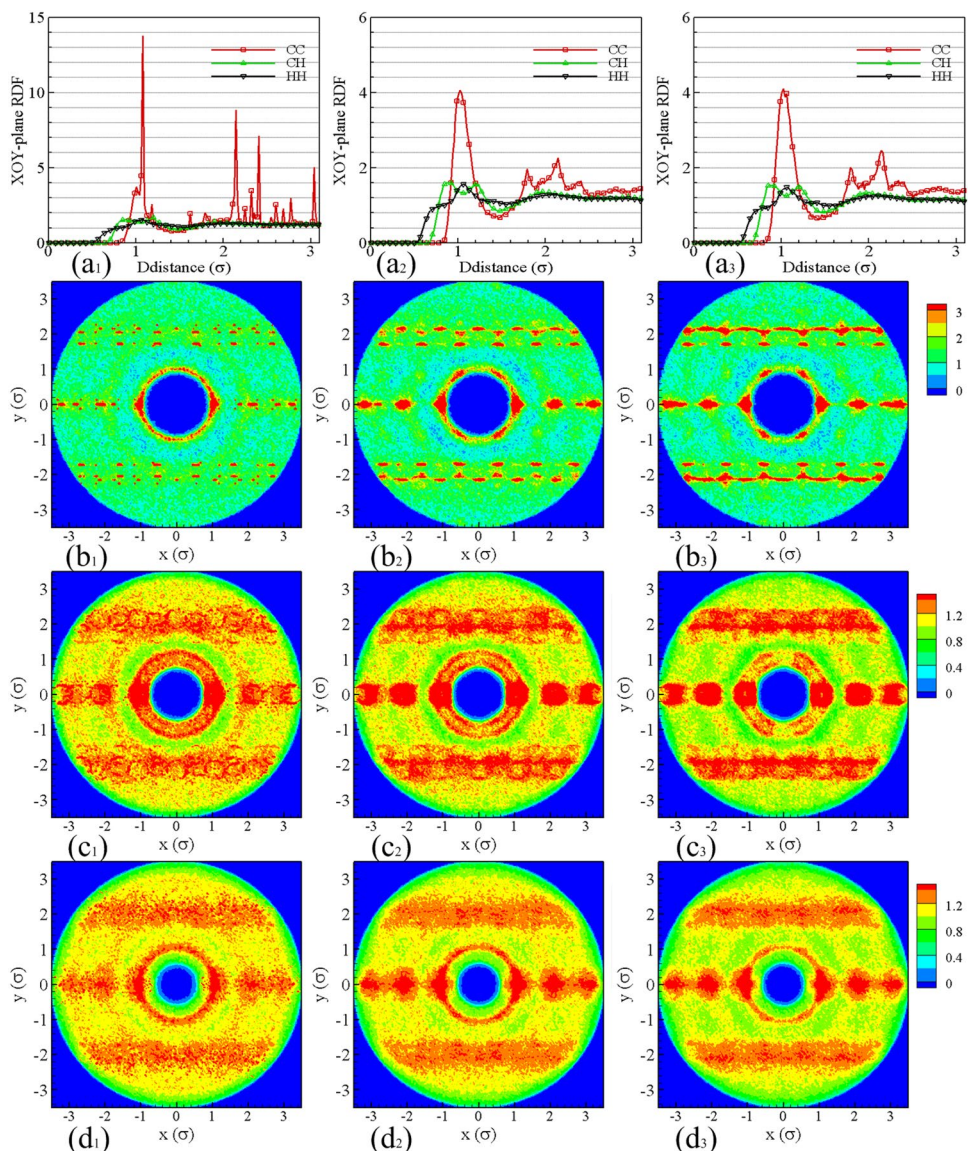


Fig. 22 The normalized velocity autocorrelation function plotted for cutoff radius over the whole channel region

of the normalized velocity autocorrelation functions gradually increase with the increasing cutoff radius. This behavior is attributed to the fact that the molecule interaction force gradually increases when cutoff radius increases. And it directly determines the moving track of molecules inside cavities. Therefore, the correlation trajectory of molecule depends on the cutoff radius. Besides, we can see from Fig. 22 that the oscillation frequency of normalized velocity autocorrelation functions has not any significant change when the cutoff radius increases or decreases. The amplitude of normalized velocity autocorrelation functions increases with the increasing cutoff radius. We attribute this behavior to the molecules suffered force at different cutoff radii. It impacts on the molecule moving trajectory. In fact, molecular trajectories remarked the diffusivity of fluid. The diffusion coefficients are calculated by the revised Green–Kubo formalism and are written as $73.52 \pm 4.12 (10^{-10} \text{ m}^2 \text{ s}^{-1})$, $69.24 \pm 1.43 (10^{-10} \text{ m}^2 \text{ s}^{-1})$, $71.05 \pm 1.37 (10^{-10} \text{ m}^2 \text{ s}^{-1})$ and $72.61 \pm 0.83 (10^{-10} \text{ m}^2 \text{ s}^{-1})$. These numerical results show that the cutoff radius has a significant impact on the diffusivity of methane Poiseuille flow, which can be explained by the nature of movement trajectories of methane molecules depending on the molecule interaction force. These simulation results indicate that the cutoff radius plays a significant role in the diffusivity of methane nanoflow moving rough nanochannel. The intermolecular interactions assume significance in the regions of rough nanochannel wall where the discrepancy appears, the diffusion coefficients only show the effect of cutoff radius on the methane fluid from the mass transfer characteristic of nanofluidic. Next, we will investigate the variation of projection radial distribution function for methane nanofluidic.

The curves and contours plotting in three planes (XOY, XOZ and YOZ), which could provide quantitative information on the distortion of the radial distribution functions [$g_{CC}(r)$, $g_{CH}(r)$ and $g_{HH}(r)$] under different cutoff radii for methane nanoflows, are presented in Figs. 23, 24, 25. It can be seen from Fig. 23, 24, 25 that the curves and contours of projections radial distribution functions [$g_{CC}(r)$, $g_{CH}(r)$ and $g_{HH}(r)$] have tiny difference when cutoff radii are not less than 2.0σ . These numerical results can be considered as the error in calculating intermolecular force from the potential. However, for $r_{\text{cut}} = 1.0 \sigma$, the projection radial distribution functions have more significant variation than that of others. This reason can be considered as the intermolecular force confined by cutoff radius. Besides, the diversity of microstructure is shown in Figs. 23, 24, and 25 on different planes. The results indicate that the cutoff radius ($r_{\text{cut}} \geq 2.0 \sigma$) does not change on the anisotropy characteristic of methane Poiseuille flow at given simulation condition. Although the present results indicate that the cutoff radius has significant impact on the microstructure of methane Poiseuille flow in nanochannel, the simulation

Fig. 23 **a₁–a₃** Total average projections of the radial distribution function [$g_{CC}(r)$, $g_{CH}(r)$ and $g_{HH}(r)$] plotted over the whole channel region in XOY plane with different cutoff radii. The contours of radial distribution function [$g_{CC}(r)$, $g_{CH}(r)$ and $g_{HH}(r)$] projected onto XOY plane [**b₁–b₃**: $g_{CC}(r)$, **c₁–c₃**: $g_{CH}(r)$ and **d₁–d₃**: $g_{HH}(r)$] plotted for different cutoff radii



results will not reflect microstructure information if the cutoff radius is too small. Thus, the cutoff radius should be properly selected for NEMSMD simulation. If a simulation is required for situations where the methane microstructure and diffusivity play vital role and cost less computational resource, $r_{cut} = 2.5 \sigma$ is recommended ($r_{cut} = 2.5 \sigma$ is used in Sects. 3.1, 3.2, 3.3).

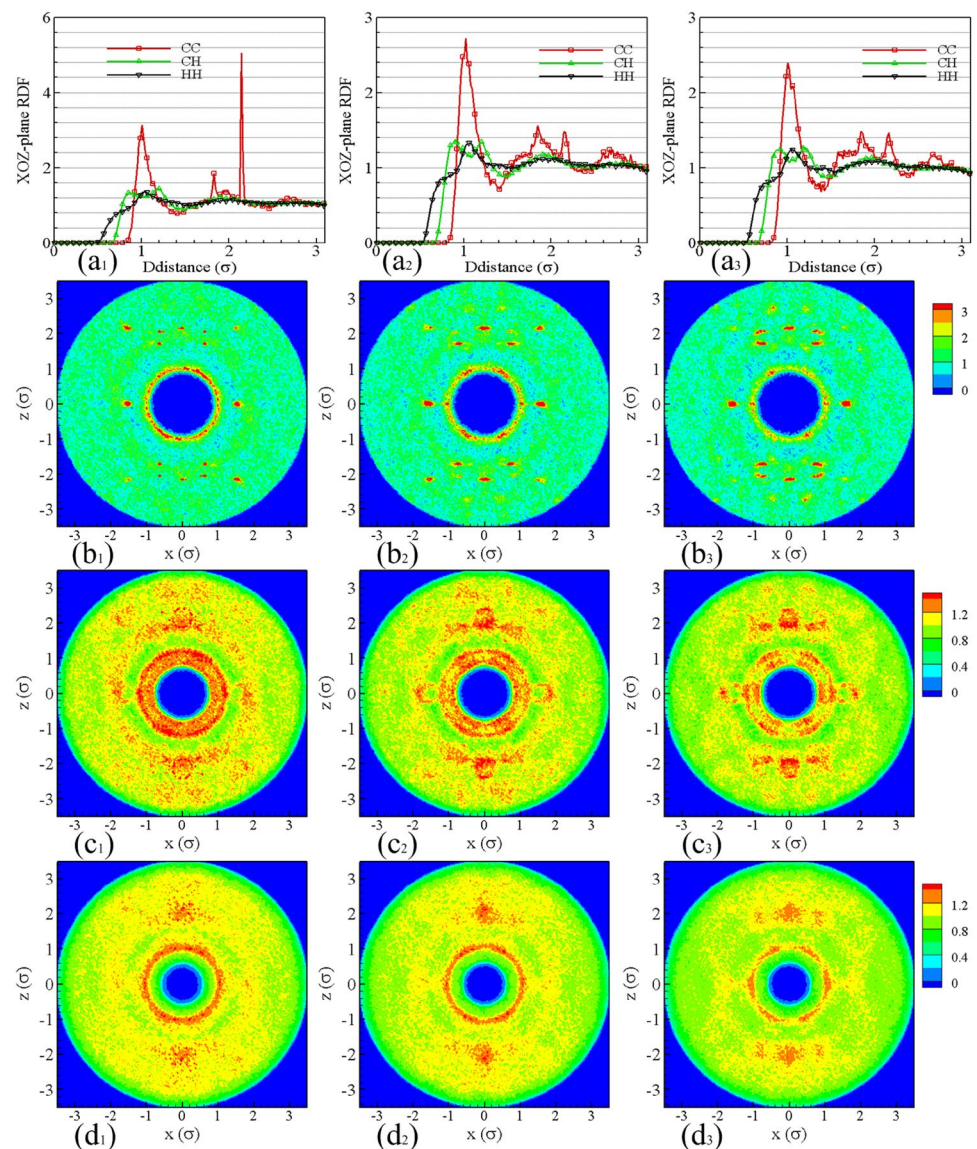
4 Conclusions

We have presented NEMSMD simulations to study microstructure and system dynamics for methane nanofluidic in rough silicon nanochannel. And the detailed research results show that the roughness, fluid–wall interaction strength, body driving force and cutoff radius have a major influence

on the microstructure information and system dynamics of methane Poiseuille flow in rough nanochannel surfaces. The main conclusions are given as:

1. The fluid–wall interaction strength, roughness wavelength, body driving force and cutoff radius have significant impact on the atoms (C and H) distribution of methane molecule. The anisotropy of methane molecule increases near nanochannel wall. Only when the methane molecules are far enough from the rough wall surface, the atoms number density distribution more or less constant is reached.
2. The fluid–wall interaction strength and roughness wavelength have obvious impact on the structure properties. Although the body driving force and cutoff radius

Fig. 24 **a₁–a₃** Total average projections of the radial distribution function [$g_{CC}(r)$, $g_{CH}(r)$ and $g_{HH}(r)$] plotted over the whole channel region in XOZ plane with different cutoff radii. The contours of radial distribution function [$g_{CC}(r)$, $g_{CH}(r)$ and $g_{HH}(r)$] projected onto XOZ plane [**b₁–b₃**: $g_{CC}(r)$, **c₁–c₃**: $g_{CH}(r)$ and **d₁–d₃**: $g_{HH}(r)$] plotted for different cutoff radii



($r_{\text{cut}} \geq 2.0 \sigma$) have no significant influence on the projection radial distribution functions (XOY-, XOZ- and YOZ plane), the anisotropy of methane molecule is presented clearly via the results of different projection planes.

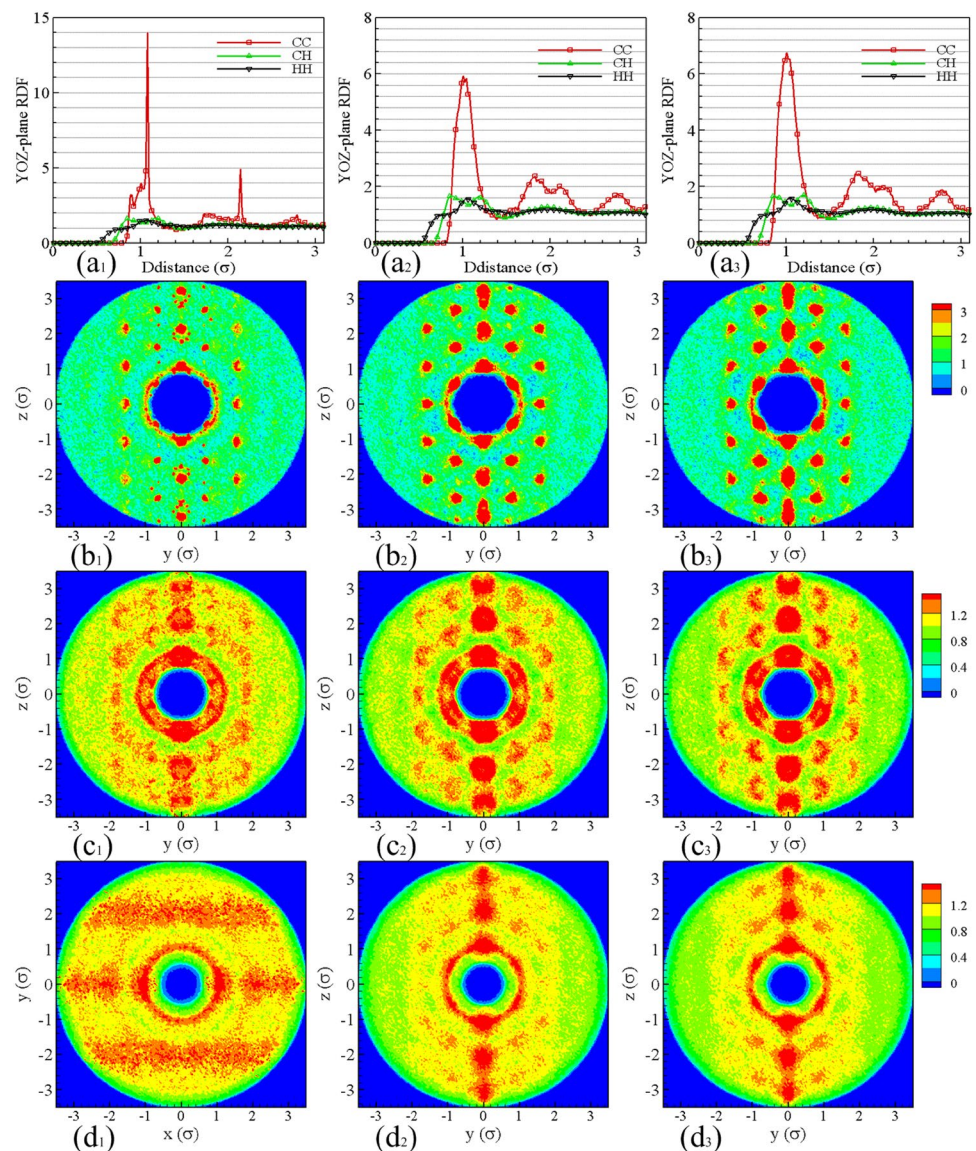
- Diffusivity has an anisotropic behavior along three different coordinate directions, since the effect of roughness of nanochannel walls [fluid–wall interaction strength, body driving force and cutoff radius ($r_{\text{cut}} \geq 2.0 \sigma$)] on the mobility of molecule at different directions. And the diffusion coefficient values increase, while wavelength [fluid–wall interaction strength, body driving force and cutoff radius ($r_{\text{cut}} \geq 2.0 \sigma$)] increases at given initial conditions.
- If a simulation is required for situations where the methane microstructure and diffusivity play vital role and

cost less computational resource; $r_{\text{cut}} = 2.5 \sigma$ is recommended.

- All these study results recommend that the surface roughness and fluid–wall interaction strength are important and should be considered in investigating the microstructures and system dynamics of methane Poiseuille flow in the rough nanochannel. It affects both mass transfer and microstructure and should be taken into consideration in energy-saving emission reduction devices.

Directions for next work, the NEMSMD framework will be used to study the significant nanofluidic system, such as methanol, binary mixture system (shale gas), Multiple mixture system (haze aerosol) and so on.

Fig. 25 **a₁–a₃** Total average projections of the radial distribution function [$g_{CC}(r)$, $g_{CH}(r)$ and $g_{HH}(r)$] plotted over the whole channel region in YOZ plane with different cutoff radii. The contours of radial distribution function [$g_{CC}(r)$, $g_{CH}(r)$ and $g_{HH}(r)$] projected onto YOZ plane [**b₁–b₃**: $g_{CC}(r)$, **c₁–c₃**: $g_{CH}(r)$ and **d₁–d₃**: $g_{HH}(r)$] plotted for different cutoff radii



Acknowledgements We are very grateful to the anonymous referees who have provided us with valuable comments and suggestions for improving our manuscript. This work is financially supported by the Science and Technology Project of Henan Province (Grant Nos. 182102210536, 182102210538), the Key Research Project of Henan Higher Education Institutions (Grant Nos. 18A120001, 18A120003, 20A110031, 20A430023, 20B130002), the National Natural Science Foundation of China (Grant No. 11671321) and Nanhu Scholars Program for Young Scholars of XYNU.

References

Bhadauria R, Aluru N (2013) A quasi-continuum hydrodynamic model for slit shaped nanochannel flow. *J Chem Phys* 139:074109

Bitsanis I, Magda JJ, Tirrell M, Davis HT (1987) Molecular dynamics of flow in micropores. *J Chem Phys* 87:1733–1750

Cao B-Y, Chen M, Guo Z-Y (2006a) Effect of surface roughness on gas flow in microchannels by molecular dynamics simulation. *Int J Eng Sci* 44:927–937

Cao B-Y, Chen M, Guo Z-Y (2006b) Liquid flow in surface-nanostructured channels studied by molecular dynamics simulation. *Phys Rev E* 74:066311

Cao B-Y, Sun J, Chen M, Guo Z-Y (2009) Molecular momentum transport at fluid-solid interfaces in MEMS/NEMS: a review. *Int J Mol Sci* 10:4638–4706

Corry B (2008) Designing Carbon Nanotube Membranes for Efficient Water Desalination. *J Phys Chem B* 112:1427

Duan C, Zhou F, Jiang K, Yu T (2015) Molecular dynamics simulation of planar Poiseuille flow for polymer melts in atomically flat nanoscale channel. *Int J Heat Mass Transf* 91:1088–1100

Hare JJ, Lammers T, Ashford MB, Puri S, Storm G, Barry ST (2016) Challenges and strategies in anti-cancer nanomedicine development: an industry perspective. *Adv Drug Deliv Rev* 108:25

- Hu C, Bai M, Lv J, Kou Z, Li X (2015) Molecular dynamics simulation on the tribology properties of two hard nanoparticles (diamond and silicon dioxide) confined by two iron blocks. *Tribol Int* 90:297–305
- Jabbarzadeh A, Atkinson J, Tanner R (2000) Effect of the wall roughness on slip and rheological properties of hexadecane in molecular dynamics simulation of Couette shear flow between two sinusoidal walls. *Phys Rev E* 61:690
- Jiang C, Ouyang J, Liu Q, Li W, Zhuang X (2016a) Studying the viscosity of methane fluid for different resolution levels models using Poiseuille flow in a nano-channel. *Microfluid Nanofluid* 20:157
- Jiang C, Ouyang J, Zhuang X, Wang L, Li W (2016b) An efficient fully atomistic potential model for dense fluid methane. *J Mol Struct* 1117:192–200
- Jiang C, Ouyang J, Li W, Wang X, Wang L (2017a) The effects of wall roughness on the methane flow in nano-channels using non-equilibrium multiscale molecular dynamics simulation. *Microfluid Nanofluid* 21:92
- Jiang C, Ouyang J, Wang L, Liu Q, Li W (2017b) Coarse graining of the fully atomic methane models to monatomic isotropic models using relative entropy minimization. *J Mol Liq* 242:1138–1147
- Jiang C, Ouyang J, Wang L, Liu Q, Wang X (2017c) Transport properties and structure of dense methane fluid in the rough nano-channels using non-equilibrium multiscale molecular dynamics simulation. *Int J Heat Mass Transf* 110:80–93
- Kamal C, Chakrabarti A, Banerjee A, Deb S (2013) Silicene beyond mono-layers—different stacking configurations and their properties. *J Phys: Condens Matter* 25:085508
- Karniadakis GE, Beskok A, Aluru N (2006) *Microflows and nanoflows: fundamentals and simulation*. Springer, New York
- Kim D, Darve E (2006) Molecular dynamics simulation of electro-osmotic flows in rough wall nanochannels. *Phys Rev E* 73:051203
- Kim H, Strachan A (2015) Effect of surface roughness and size of beam on squeeze-film damping—Molecular dynamics simulation study. *J Appl Phys* 118:204304
- Kong CL (1973) Combining rules for intermolecular potential parameters. II. Rules for the Lennard-Jones (12–6) potential and the Morse potential. *J Chem Phys* 59:2464–2467
- Li Y, Chen D, Zhang Y, Liu C, Chen P, Wang Y, Feng X, Du W, Liu BF (2016) High-throughput single cell multidrug resistance analysis with multifunctional gradients-customizing microfluidic device. *Sens Actuators B Chem* 225:563–571
- Liakopoulos A, Sofos F, Karakasidis TE (2016) Friction factor in nano-channel flows. *Microfluid Nanofluid* 20:1–7
- Mantzalis D, Asproulis N, Drikakis D (2011) Filtering carbon dioxide through carbon nanotubes. *Chem Phys Lett* 506:81–85
- Markesteyn A, Hartkamp R, Luding S, Westerweel J (2012) A comparison of the value of viscosity for several water models using Poiseuille flow in a nano-channel. *J Chem Phys* 136:134104
- Mashayak S, Aluru N (2012a) Coarse-grained potential model for structural prediction of confined water. *J Chem Theory Comput* 8:1828–1840
- Mashayak S, Aluru N (2012b) Thermodynamic state-dependent structure-based coarse-graining of confined water. *J Chem Phys* 137:214707
- Mo G, Rosenberger F (1990) Molecular-dynamics simulation of flow in a two-dimensional channel with atomically rough walls. *Phys Rev A* 42:4688
- Morris JF (2009) A review of microstructure in concentrated suspensions and its implications for rheology and bulk flow. *Rheol Acta* 48:909–923
- Noid W (2013) Perspective: coarse-grained models for biomolecular systems. *J Chem Phys* 139:090901
- Noorian H, Toghraie D, Azimian A (2014) The effects of surface roughness geometry of flow undergoing Poiseuille flow by molecular dynamics simulation. *Heat Mass Transf* 50:95–104
- Priezjev NV (2007) Effect of surface roughness on rate-dependent slip in simple fluids. *J Chem Phys* 127:144708
- Ranjith SK, Patnaik B, Vedantam S (2013) No-slip boundary condition in finite-size dissipative particle dynamics. *J Comput Phys* 232:174–188
- Rapaport DC (2004) *The art of molecular dynamics simulation*. Cambridge University Press, Cambridge
- Sharma AK, Tiwari AK, Dixit AR (2016) Rheological behaviour of nanofluids: a review. *Renew Sustain Energy Rev* 53:779–791
- Shell MS (2008) The relative entropy is fundamental to multiscale and inverse thermodynamic problems. *J Chem Phys* 129:108
- Sofos F, Karakasidis T, Liakopoulos A (2009a) Variation of transport properties along nanochannels: a study by non-equilibrium molecular dynamics. *IUTAM Symposium on Advances in Micro- and Nanofluidics*. Springer, Netherlands, pp 67–78
- Sofos FD, Karakasidis TE, Liakopoulos A (2009b) Effects of wall roughness on flow in nanochannels. *Phys Rev E* 79:026305
- Sofos F, Karakasidis TE, Liakopoulos A (2010) Effect of wall roughness on shear viscosity and diffusion in nanochannels. *Int J Heat Mass Transf* 53:3839–3846
- Sofos F, Karakasidis TE, Liakopoulos A (2012) Surface wettability effects on flow in rough wall nanochannels. *Microfluid Nanofluid* 12:25–31
- Sofos F, Karakasidis TE, Liakopoulos A (2015) Fluid structure and system dynamics in nanodevices for water desalination. *Desalination Water Treat* 57:1–11
- Sofos F, Karakasidis TE, Giannakopoulos AE, Liakopoulos A (2016) Molecular dynamics simulation on flows in nano-ribbed and nano-grooved channels. *Heat Mass Transf* 52:153–162
- Sundar LS, Sharma KV, Singh MK, Sousa ACM (2017) Hybrid nanofluids preparation, thermal properties, heat transfer and friction factor—a review. *Renew Sustain Energy Rev* 68:185–198
- Wang J, Chen DR, Pui DYH (2015) Modeling of filtration efficiency of nanoparticles in standard filter media. *J Nanopart Res* 9:109–115
- Zhang Y (2016a) Effect of wall surface modification in the combined Couette and Poiseuille flows in a nano channel. *Int J Heat Mass Transf* 100:672–679
- Zhang Y (2016b) Effect of wall surface roughness on mass transfer in a nano channel. *Int J Heat Mass Transf* 100:295–302

Publisher's Note Springer Nature remains neutral with regard to jurisdictional claims in published maps and institutional affiliations.